Scientific Research Publishing

Open Journal of Geology, 2023, 13, 107-135
https://www.scirp.org/journal/ojg
ISSN Online: 2161-7589
ISSN Print: 2161-7570

Geochemistry and Petrogenesis of Basic and Ultrabasic Rocks Elogo Complex in Ivindo Archean Block (Congo Craton): Geodynamic Implications

Nelson Lekeba Makamba[1,2*], Vicky Tendresse Télange Bouenitela[1], Ulrich Verne Matiaba-Bazika[1,2], Florent Boudzoumou[1,2]

[1]Geodynamics Laboratory, Faculty of Science and Technology, Marien Ngouabi University, Brazzaville, Republic of the Congo
[2]Department of Geosciences, National Institute for Research in Exact and Natural Sciences, Brazzaville, Republic of the Congo
Email: *nelson.makamba.27@gmail.com, Vicky_bouenitela@yahoo.fr, iletbazika@gmail.com, boudzoumouf@gmail.com

How to cite this paper: Makamba, N.L., Bouenitela, V.T.T., Matiaba-Bazika, U.V. and Boudzoumou, F. (2023) Geochemistry and Petrogenesis of Basic and Ultrabasic Rocks Elogo Complex in Ivindo Archean Block (Congo Craton): Geodynamic Implications. *Open Journal of Geology*, **13**, 107-135.
https://doi.org/10.4236/ojg.2023.132006

Received: October 4, 2022
Accepted: February 7, 2023
Published: February 10, 2023

Abstract

The Elogo complex is a greenstone belt portion located on the Eastern edge of the Archean Congo craton at the junction with the Paleoproterozoic to Neoproterozoic Sembe Ouesso basin. This study was carried out on this complex to determine the context of the placement of basaltic rocks. Metaluminous tholeiitic basalts (basic and ultrabasic), calc-alkaline basalts, andesitic basalts, and peraluminous calc-alkaline dacites represent greenstones. Tholeiitic and calc-alkaline basalts come from deep enriched and depleted mantle sources, including garnet in fusion residues [Al_2O_3/TiO_2 > 16 (16.5 to 35.12) and in some samples between 12.45 to 14.48; CaO/Al_2O_3 < 1 (0.52 to 0.97) and >1 (1.04 to 1.35) in ten samples and $(Gb/Yb)_{PM}$ > 1]. The calc-alkaline dacites come from a shallow depleted mantle source [Al_2O_3/TiO_2 > 16; CaO/Al_2O_3 < 1 and $(Gb/Yb)_{PM}$ > 1]. Tholeiitic and calc-alkaline basalts have a negative Rb, Ba, Ce, and Nb anomaly without negative Ti anomaly, positive Ta, Pb anomalies, and a lack of significant REE [(La/Yb)n = 0.36 to 0.97 and 1 to 2.15; (Ce/Yb)n = 0.27 to 0.96 and 1.04 to 1.72, respectively] fractionation. High Nb/Th (2 to 10) and Nb/U (1.82 to 26) ratios and low La/Ta (5 to 27) ratios are characteristic of divergent margin magmatic sources. Tholeiitic and calc-alkaline basalts correspond to an extensive back-arc basin-type tectonic setting. Calc-alkaline andesitic basalts and dacites show positive Ba, U, Th, K, La, Ce, Pb, and Li anomalies and negative Nb, Ta, and Ti anomalies reflecting crustal contamination and hydrothermal alteration in a compressive tectonic context as a volcanic arc in a subduction regime marking the interruption of the meso-neoarchean Elogo's opening. Elogo's opening and closing are probably as-

sociated with the emplacement of the greenstone of the meso-neoarchean Gabon Belinga group and the relics of the Mesoarchean greenstones of the Cameroun Ntem complex.

Keywords

Elogo, Greenstone, Archean, Tholeiitic, Andesitic Basalts, Dacites, Magma Source

1. Introduction

In western central Africa, the rocks of the Congo craton outcrop in Congo, Gabon, and Cameroon. In the northwest of the Congo, rocks of the Archean age form the Ivindo Archean Block (IAB) up to Gabon and the Ntem complex in southern Cameroon (**Figure 1**) [1] [2].

The IAB is like other known archean cratons in various places in Africa and elsewhere (West African, Kalahari, Sao Francisco cratons), composed of various sequences of migmatitic granito-gneiss associated with greenstone belts of various dimensions. The granitoïdes are composed in this western part of the Congo craton of charnockites, tonalites, granodiorites, diorites, trondhjemites and syenogranites [3] [4] [5] [6]. In the IAB in Congo, greenstone belts are known in Badondo, Avima, Nabeba, Egbala mounts, and the Elogo region. The best-studied Belinga greenstone belt found in Gabon led to the definition of the Belinga group [4]. These belts are composed of ultrabasic rocks, amphibole-pyroxene rich rocks, amphibolite, chlorite-sericite-schists, talc schists, and banded iron formations. These formations are metamorphosed into greenschist and amphibolite facies. Greenstone belts are geological markers contributing to the geodynamic knowledge of the emplacement of known Archean cratons. They trace the magmatic properties of the mantle sources (composition, genetic temperature) up to 3.8 Ga [7] [8] [9]. In Congo, only some published studies are devoted to greenstone belts. The work often focuses on the BIF [2] [10] associated with these green rocks, which form iron deposits that are currently relatively well-mapped and are the subject of economic projects. The present study relates to the Elogo-Bamegod zone, where outcrops basic-ultrabasic rocks called the "Elogo Complex". The work is focused on the petrology and geochemistry of the basic rocks sampled in these localities. The geochemistry of basic rocks allows the construction of affinities and magmatic sources and the evaluation of crust-mantle interactions to reconstruct the geodynamic context of their formation and related processes.

2. Geological Setting

The Elogo-Bamegod area represents one of the regions where outcrop rocks forming greenstone belts are distributed in the IAB (**Figure 2(A)**) attached to the Congo craton. It occupies the eastern portion of the greenstone belt of the locality and is overlain in major unconformity by the Paleoproterozoic to the

Neoproterozoic cover of the Sembe-Ouesso basin. In the north of this locality, the granitoids are formed of charnockites, tonalites/granodiorites, and peraluminous, calc-alkaline trondhjemites, relatively rich in sodium, dated between 3.23 Ga and 2.7 Ga and placed in a conceptual model of continental crust evolution [5].

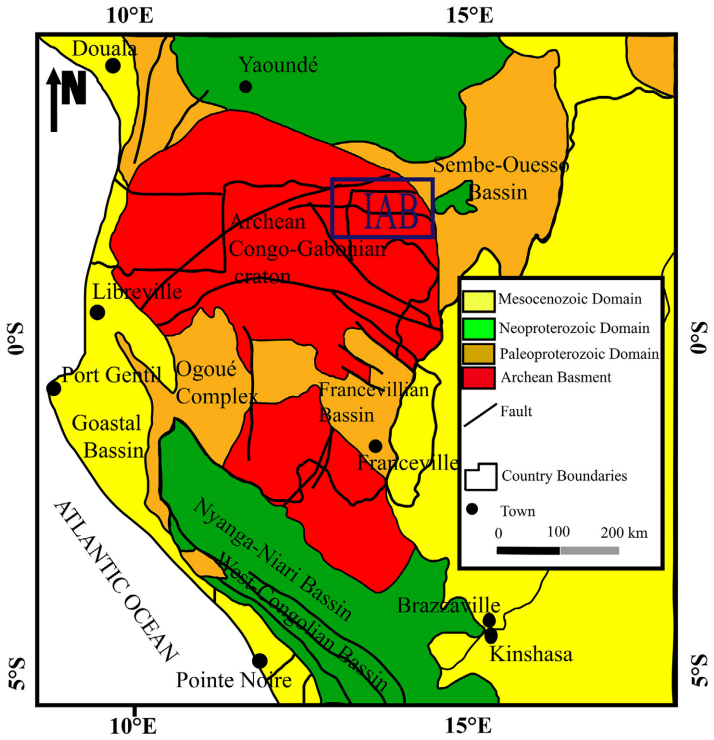

Figure 1. Simplified regional geological map of the Archean Congo-Gabonian Craton with the location of studied areas (IAB: Ivindo Archean Block) modified from [1] [2].

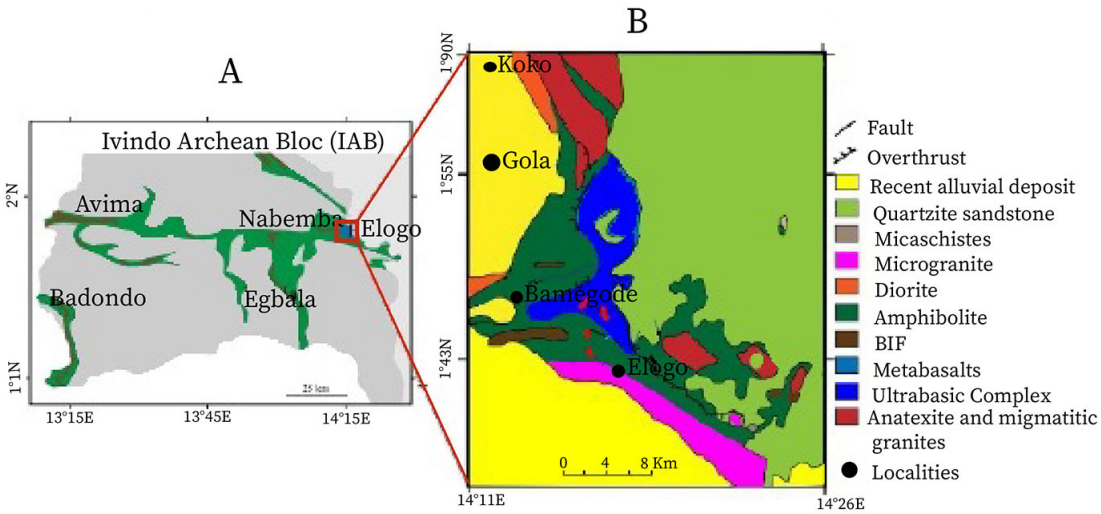

Figure 2. Cartographic maps: A—of Ivindo Archean Block (IAB) after [2]; B—expanded area of the Elogo ultrabasic Complex modified from the Geological map of Ivindo basement of BRGM. Red points = tholeiitic basalts; blue points = basalts and calc-alkaline andesitic basalts, black points = calc-alkaline dacites.

In the Elogo area, granito-gneiss (**Figure 2(B)**) are composed of anatectic, migmatitic granites, diorites, microgranites, gneiss and migmatites in amphibolite to granulite metamorphic facies. The greenstone belt comprises metabasalts, amphibolites, undifferentiated basic and ultrabasic rocks, micaschists, quartzites, and BIF. They locally show East verging folds, accompanied by penetrative crenulation schistosity mainly oriented NNW-SSE, and often masking the flow schistosity. Further to the East, the formations are affected by the eastern vergence thrust. The Elogo-Bamegod zone is affected by a major shear-oriented E-W with locally associated shears more or less NNW-SSE to NNE-SSW.

3. Samples Material and Analytical Method

3.1. Samples Material

The greenstone samples were taken from the river banks, hills flanks, and artificial banks located at Elogo and Bamegod and mapped as Elogo complex. Thin sections were made on well selected samples.

3.2. Analytical Method

Geochemical analyses of major, trace and rare earth elements (REE) were done to evaluate the petrogenesis of rocks. Samples were analyzed in the ALS laboratory of Canada according to ALS protocol. Quality control is realized with international geostandards. Major, Ba, Cr, Sc, and trace elements are analyzed by ICP-AES. The rest of the trace and the rare earth elements were analyzed by ICP-MS. Total C and total S were determined using a LEXO analyzer.

4. Results

4.1. Macroscopic Description

The metabasite rocks outcrop widely in rivers (Ebeck, Maziézié, Melaba, Kampala, Guinée, Namoumédia), in some mountains, and on artificial slopes. They are composed of the most abundant amphibolites, chlorite schists, and epidotes. They appear in massive form with little penetrable schistosity, in the form of levels with strongly penetrable schistosity or gneissified and/or migmatized. Folds accompanied by flow schistosity (S1) and crenulation (S_2) are locally visible (**Figure 3**). Fracture planes intersecting the schistosity are present and determine strongly developed shears-oriented E-W to N-S, sometimes NE-SW.

4.2. Microscopic Description

Twenty-eight (28) thin sections were made from samples of amphibolites, chlorite schists, and epidotes, which are studied under an optical microscope (**Figure 4**).

Amphibolites come in several compositions with the presence or absence of mineralogical varieties as well as their abundance. They are represented by samples Kamp 107 and 81, Mela 96 and Nam 43c. Sample Kamp 107 is composed of tremolite, brown hornblende, actinote, magnetite, and spinel with some chloritized or carbonatized hornblendes. The texture is nematoblastic. Sample Kamp

81 contains tremolite, brown hornblende, actinote, chlorite, epidote and opaque minerals with nematoblastic texture. Sample Mela 96 is made of brown and green hornblende, tremolite, actinote, epidote, chlorite and plagioclase with nematoblastic texture. Sample Nam 43c comprises porphyroblastic hornblendes disseminated in a microlitic matrix of biotite, epidote, chlorite, quartz, plagioclase, carbonate, and sulfide (**Figure 4(A)**).

Chlorite schists are often in contact with amphibolites and are represented in samples Maz 183b and Mela 101. Sample Maz 183b is composed of chlorite, muscovite, calcite, quartz, talc and opaque minerals with a lepido-granoblastic texture. Sample Mela 101 is composed of chlorite, calcite, quartz, cordierite, muscovite, rutile, sulpfide and hematite, with lepidoblastic texture. Epidotite is represented by samples Mela 103b and Bam 12. They were sampled in the locality of Bamegod. Sample Mela 103b is made of epidote, chlorite, calcite, cordierite, muscovite, plagioclases and rutile with lepido-granoblastic texture. Sample Bam 12 contains a large portion of the epidote cluster (pistachite) associated with actinote, tremolite, muscovite, zoisite, and opaque minerals in a granoblastic texture (**Figure 4(B)**).

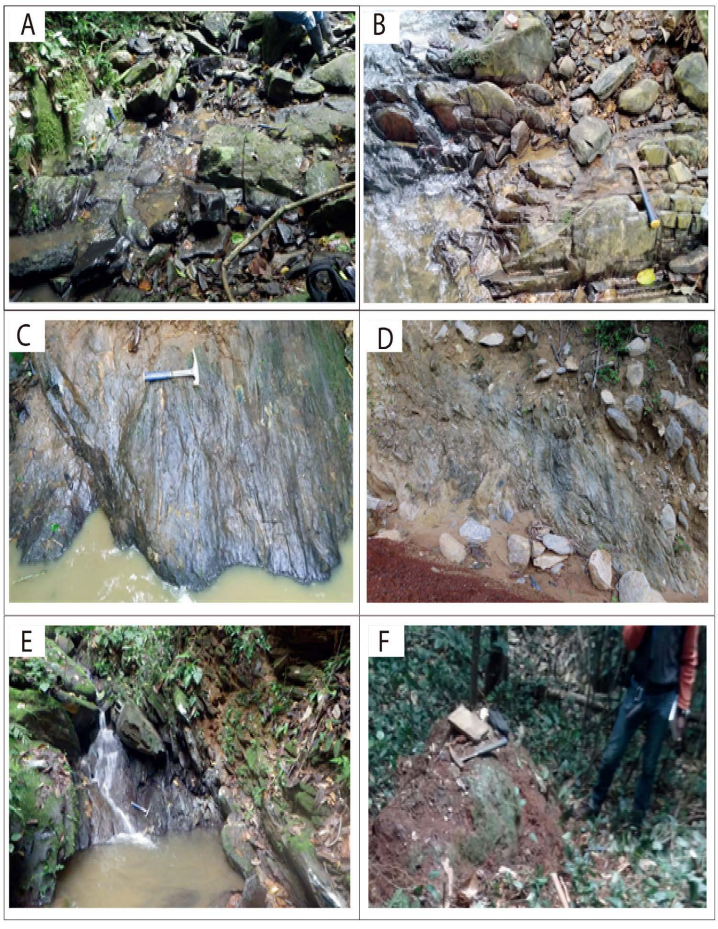

Figure 3. Examples of some basic rocks outcropping in Elogo-Bamegode area; A, B—Massive amphibolite with strong fracturation; C—Amphibolite with crenulation schistosity, D, E—Chlorite schists with crenulation schistosity, F—Altered epidote.

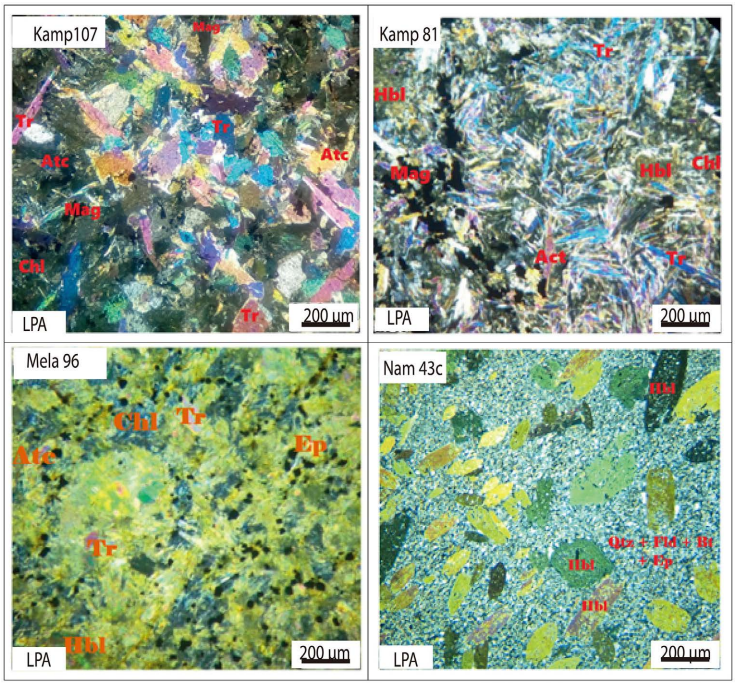

A

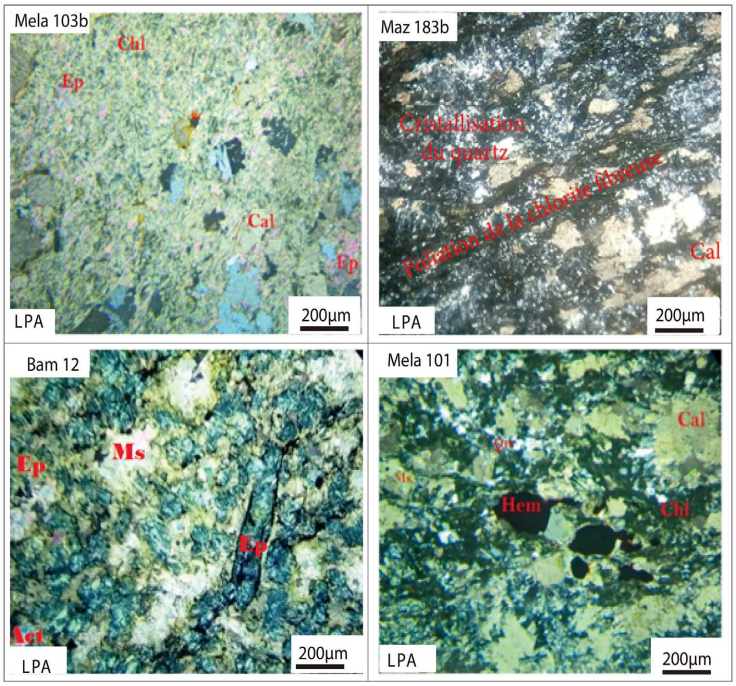

B

Figure 4. Microscopic photography of amphibolites, chlorite schists, and epidotes from Elogo complex. A: Basic and ultrabasic amphibolites (Kamp 107 and 81, Mela 96), and hydrothermal circulation (Nam 43c). B: Basic and ultrabasic chlorite schists (Mela101, Maz 183) and epidotes (Mela 103b and Bam 12). Bt-biotite, Cal-calcite, Chl-chlorite, Crd-cordierite, Ep-epidote, Hbl-hornblende, Hem-hematite, Om-opaque, mineral, Mag-magnetite, Pl-plagioclase, Qtz-quartz, R-Qtz Quartz recrystallisation, Rt-rutile, Tr-tremolite.

4.3. Geochemistry and Petrology Classification

Twenty-eight (28) samples of amphibolites, chlorite schists and epidotes from the Elogo complex are analyzed. Their results are presented in Table 1. The SiO_2 is comprised of between 37.50% and 68.40% values. Al_2O_3 varies from a low value of 2.74% to a high value of 15.60%. Fe_2O_3 is situated from 5.99% to 13.65%, MgO is comprised between 2.75% to 25.5%, CaO varies from 3.01% to 11.20%, Na_2O is between 0.01% and 3.75% with one sample contains less of 0.01%, K_2O has a value comprised between 0.01% and 2.31% with three samples showing less of 0.01%, MnO varies from 0.09 and 0.22, P_2O_5 is comprised between 0.01 and 0.40 and TiO_2 is situated from 0.12% to 1.13%. The LOI is low (0.85%) to medium (1.13% to 1.53%) in a few samples and very high in most samples, reaching up to 16.4% and confirming a strong hydrothermal and/or metamorphic alteration observed in the field, despite the possible hydrothermal or metamorphism alteration $Na_2O + K_2O$ vs. SiO_2 diagram of TAS [11] plot the major rocks in sub alkaline tholeiitic basalt, a few samples in dacite and a rare sample in basaltic andesite (Figure 5(A)). In the AFM diagram of [12], the samples are mostly in the tholeiitic series, although far from the line of separation of the calc-alkaline field. Two samples are, however, in this last field. In addition, all basic and ultrabasic rocks are plotted in the tholeiitic basalt field. (Figure 5(B)).

Table 1. Composition of major elements (%) and traces (ppm) of basalts and dacites of Elogo complex.

Rocks type	**Tholeiiticbasalts**													
Sample	Guin 77	Guin 78	Kam 08	Kam 15	Kam 69	Kam81b	Bam 12	Bam 14	Mel 154	Mel 157	Ebek160	Ebek161	Ebek165	Ebek169
SiO_2	41.30	45.40	44.60	44.80	42.00	47.40	44.60	45.60	38.10	41.60	41.90	42.90	46.10	41.50
Al_2O_3	5.94	6.35	7.90	5.69	7.67	5.88	4.81	5.55	6.15	6.82	6.02	6.60	4.58	4.17
Fe_2O_3	13.25	9.97	11.7	10.50	13.20	10.45	10.65	10.95	9.49	9.14	9.95	11.4	9.33	9.95
CaO	7.00	6.87	6.57	6.98	5.80	7.54	5.95	7.00	8.31	7.08	4.68	6.37	7.70	4.76
MgO	22.20	21.90	21.30	22.8	22.00	22.50	24.20	23.50	18.70	18.20	26.00	23.80	24.00	25.50
Na_2O	0.26	0.20	0.42	0.41	0.31	0.42	0.42	0.24	0.92	1.68	0.32	0.45	0.60	0.01
K_2O	0.01	0.02	0.05	0.14	0.04	0.04	0.19	0.08	0.09	<0.01	<0.01	0.01	0.02	<0.01
Cr_2O_3	0.397	0.319	0.344	0.404	0.324	0.288	0.33	0.326	0.267	0.285	0.305	0.342	0.318	0.306
TiO_2	0.41	0.26	0.36	0.26	0.41	0.32	0.29	0.30	0.32	0.28	0.31	0.31	0.14	0.24
MnO	0.19	0.16	0.18	0.18	0.17	0.18	0.17	0.15	0.16	0.15	0.18	0.15	0.15	0.19
P_2O_5	0.02	0.01	0.40	<0.01	0.05	<0.01	<0.01	<0.01	0.02	0.02	0.05	<0.01	0.01	0.01
SrO	<0.01	<0.01	<0.01	<0.01	<0.01	<0.01	<0.01	<0.01	0.01	0.01	<0.01	<0.01	<0.01	<0.01
BaO	<0.01	<0.01	<0.01	<0.01	<0.01	<0.01	<0.01	<0.01	<0.01	<0.01	<0.01	<0.01	<0.01	<0.01
LOI	6.27	12.70	7.93	6.54	7.34	6.60	6.88	6.73	6.94	5.58	0.85	1.13	8.81	7.27
Total	**99.22**	**99.34**	**98.91**	**98**	**100.8**	**98.76**	**98.56**	**100.43**	**98.91**	**100.6**	**100.86**	**100.11**	**98.53**	**99.6**
Cr	3080	2510	2680	3110	2660	2180	2290	2470	1960	2070	2290	2490	2360	2300
Ni	1480	1160	1110	1290	1080	1100	1320	1230	1020	1060	1430	1350	1280	1540

Continued

Rb	0.40	0.40	0.60	0.40	0.40	0.30	0.80	0.30	0.30	0.40	0.60	0.60	1.10	0.20
Sr	27.00	12.00	12.30	9.50	9.10	12.60	19.20	9.00	86.30	73.70	13.40	15.90	23.60	21.20
Cs	0.17	0.04	0.06	0.09	0.07	0.07	0.77	0.12	0.05	0.05	0.15	0.10	0.31	0.03
Ba	3.80	5.10	16.40	12.00	2.90	7.90	4.60	4.90	4.00	2.80	4.30	3.70	17.60	1.40
Sc	34.00	21.00	23.00	22.00	29.00	23.00	21.00	22.00	20.00	19.00	18.00	23.00	21.00	15.00
V	168	116	159	140	177	122	86	140	124	61	108	110	59	100
Hf	0.50	0.50	0.70	0.40	1.00	0.60	0.60	0.40	0.60	0.70	0.40	0.60	0.50	0.30
Nb	0.60	0.40	0.50	0.40	0.60	1.30	0.50	0.70	1.00	0.30	0.50	0.40	0.20	0.30
Zr	15.00	18.00	24.00	14.00	32.00	22.00	16.00	15.00	21.00	16.00	7.00	15.00	11.00	14.00
Ta	0.10	0.10	0.10	0.10	0.10	0.20	0.10	0.10	0.10	0.10	0.10	0.10	0.10	0.10
Th	0.17	0.06	0.11	0.19	0.12	0.24	0.07	0.09	0.25	0.15	<0.05	0.07	0.09	0.06
U	<0.05	<0.05	<0.05	<0.05	<0.05	0.05	<0.05	<0.05	0.06	<0.05	<0.05	<0.05	0.11	<0.05
Y	9.30	5.40	7.00	5.00	7.70	8.00	8.50	9.10	7.60	3.50	4.70	6.80	5.60	5.50
La	0.90	1.30	0.80	0.80	0.80	1.30	0.60	0.90	1.20	0.70	0.80	1.40	1.40	0.40
Ce	1.90	2.20	2.80	1.60	2.40	3.00	1.50	2.00	2.80	1.60	1.00	1.10	1.90	1.20
Pr	0.30	0.34	0.40	0.28	0.41	0.51	0.25	0.39	0.40	0.25	0.33	0.50	0.35	0.23
Nd	1.70	1.60	1.80	1.40	2.30	2.40	1.60	2.10	1.80	1.40	1.17	2.30	17.00	1.30
Sm	0.82	0.72	0.72	0.54	1.00	0.99	0.67	1.10	0.72	0.48	0.54	0.92	0.64	0.53
Eu	0.24	0.12	0.22	0.13	0.10	0.27	0.20	0.26	0.27	0.17	0.20	0.27	0.26	0.21
Gd	1.49	0.88	1.08	0.89	1.46	1.26	1.05	1.20	1.13	0.75	0.95	1.19	0.98	0.81
Tb	0.24	0.19	0.20	0.14	0.26	0.22	0.17	0.27	0.21	0.11	0.15	0.22	0.17	0.14
Dy	1.61	1.12	1.40	0.93	1.63	1.65	1.33	1.66	1.57	0.70	0.97	1.53	1.18	0.92
Ho	0.29	0.22	0.32	0.20	0.33	0.30	0.28	0.34	0.29	0.14	0.18	0.31	0.23	0.21
Er	0.88	0.59	0.81	0.60	0.79	1.04	0.94	0.90	0.93	0.39	0.61	0.88	0.66	0.55
Tm	0.11	0.10	0.11	0.10	0.11	0.14	0.13	0.15	0.14	0.06	0.08	0.11	0.09	0.07
Yb	0.83	0.52	0.79	0.63	0.89	0.94	0.76	0.92	0.93	0.44	0.40	0.74	0.48	0.53
Lu	0.11	0.07	0.09	0.10	0.10	0.13	0.11	0.10	0.11	0.05	0.07	0.13	0.07	0.06
Pb	2	<2	<2	5	<2	<2	<2	4	2	<2	2	<2	2	2

Rocks type	**Tholeiiticbasalts**				**Basalt and calc-alkaline andesitic basalts**				**Calc-alkaline dacites**					
Sample	Mel 95	Mel 96	Mel 100	Mel 101	Mel103A	Maz 186	Maz 188	Maz 191	Nam 32	Nam41a	Nam41e	Nam43c	Nam60	Nam67
SiO_2	43.20	45.00	40.80	40.90	43.40	37.50	43.90	53.10	66.00	65.20	50.20	68.40	50.70	50.40
Al_2O_3	6.36	6.48	6.99	7.35	6.31	9.20	12.75	2.74	14.45	14.05	15.60	14.05	13.95	15.25
Fe_2O_3	11.85	12.20	11.00	9.12	10.35	11.00	8.94	8.50	6.98	7.270	12.70	5.99	13.65	11.20
CaO	5.83	6.79	6.85	7.98	5.45	5.95	6.69	10.95	3.06	3.01	10.15	3.17	10.55	11.20
MgO	23.50	23.00	20.20	16.00	20.60	17.45	8.45	20.20	3.21	2.93	5.36	2.75	6.96	7.68
Na_2O	0.26	0.51	0.29	1.38	0.99	<0.01	0.98	0.09	3.75	2.94	2.21	3.34	2.03	2.23
K_2O	0.02	0.06	0.02	0.03	0.03	0.08	1.71	0.03	2.07	2.31	1.25	1.77	0.66	0.53

Continued

Cr_2O_3	0.356	0.369	0.375	0.233	0.309	0.248	0.066	0.098	0.035	0.034	0.018	0.031	0.039	0.049
TiO_2	0.32	0.38	0.37	0.37	0.35	0.42	0.59	0.12	0.48	0.44	1.13	0.40	1.12	0.63
MnO	0.15	0.16	0.11	0.15	0.16	0.14	0.15	0.16	0.10	0.11	0.20	0.09	0.22	0.16
P_2O_5	0.02	0.01	0.02	0.03	0.03	0.03	0.06	0.01	0.14	0.10	0.09	0.10	0.10	0.03
SrO	<0.01	<0.01	0.01	0.01	<0.01	<0.01	0.01	<0.01	0.05	0.06	0.02	0.05	0.02	0.01
BaO	<0.01	<0.01	<0.01	<0.01	0.01	<0.01	0.03	<0.01	0.12	0.07	0.02	0.06	0.01	<0.01
LOI	7.19	6.76	11.55	15.90	12.40	13.30	16.40	15.15	13.7	3.42	1.40	1.47	1.18	1.53
Total	**99.06**	**101.72**	**98.59**	**99.45**	**100.39**	**98.57**	**98.94**	**97.17**	**98.03**	**99.42**	**101.85**	**99.99**	**100.13**	**101.73**
Cr	2630	2500	2500	1600	2060	1660	470	720	240	240	120	210	280	360
Ni	1360	1310	1145	819	1195	584	108	657	123	132	94.00	125	128	83
Rb	0.40	0.50	0.30	0.20	0.20	0.30	59.00	0.70	57.50	77.40	52.60	63.00	25.40	25.00
Sr	9.50	19.30	62.90	74.00	39.70	17.90	44.80	4.60	418	459	198	393	136	111.50
Cs	0.04	0.25	0.06	0.03	0.04	0.09	1.62	0.09	3.72	4.75	2.97	3.68	2.12	1.68
Ba	3.00	3.50	8.30	2.10	77.50	6.90	300	4.00	1040	584	190	479	123	38.7
Sc	26.00	24.00	23.00	19.00	21.00	24.00	28.00	8.00	3.72	4.75	2.97	3.68	2.12	1.68
V	137	129	105	111	103	118	185	69.00	98.00	80.00	268	74.00	301	253
Hf	0.50	0.70	0.70	0.90	0.60	1.10	1.80	0.60	3.10	3.60	2.60	2.90	2.00	1.50
Nb	0.30	0.50	0.90	1.20	0.60	1.40	3.30	0.50	4.70	4.00	3.70	3.70	3.10	2.20
Zr	14.00	21.00	22.00	31.00	19.00	30.00	61.00	13.00	107	118	81.00	94.00	69.00	48.00
Ta	0.10	0.10	0.10	0.10	0.10	0.20	0.20	0.20	0.50	0.40	0.30	0.40	0.30	0.20
Th	<0.05	0.09	0.15	0.49	0.10	0.30	0.98	0.24	6.86	4.96	1.75	5.00	1.47	0.37
U	<0.05	<0.05	0.08	0.14	<0.05	0.42	0.41	0.05	1.95	1.47	0.58	1.41	0.36	0.10
Y	6.80	10.90	6.10	8.10	9.40	11.90	20.80	10.2	13.6	9.60	24.7	10.70	24.50	19.00
La	0.50	1.30	1.40	2.60	0.50	2.90	5.30	2.60	27	21.80	8.10	21.80	7.70	3.40
Ce	0.80	2.00	3.50	6.10	1.40	6.10	11.80	1.90	46.6	38.30	16.6	39.10	15.90	8.60
Pr	0.24	0.48	0.55	0.83	0.21	0.92	1.70	1.37	5.51	4.38	2.23	4.47	2.09	1.38
Nd	1.50	2.40	2.40	3.30	1.20	4.20	8.30	5.8	20.8	17.00	10.10	17.30	10.00	6.90
Sm	0.61	0.85	0.72	0.89	0.47	1.25	2.27	1.73	3.74	2.70	3.16	2.75	3.02	2.08
Eu	0.23	0.39	0.14	0.26	0.17	0.44	1.00	0.55	1.05	0.80	0.97	0.85	0.99	0.78
Gd	1.12	1.71	0.95	1.41	1.27	1.92	3.23	1.97	2.72	2.40	4.13	2.43	3.91	3.93
Tb	0.20	0.27	0.18	0.13	0.24	0.37	0.57	0.43	0.4	0.36	0.67	0.31	0.67	0.53
Dy	1.34	1.69	1.15	1.53	1.79	2.15	3.82	2.51	2.68	1.73	4.50	1.94	4.63	3.46
Ho	0.27	0.38	0.23	0.32	0.33	0.47	0.80	0.49	0.48	0.38	0.96	0.38	0.88	0.68
Er	0.86	1.13	0.75	0.96	0.98	1.26	2.33	1.48	1.19	0.95	2.81	1.03	2.65	2.08
Tm	0.11	0.16	0.08	0.12	0.15	0.18	0.32	0.17	0.16	0.13	0.38	0.14	0.34	0.30
Yb	0.77	0.91	0.63	0.83	0.95	1.26	2.24	1.63	1.11	0.92	2.56	1.00	2.44	2.12
Lu	0.09	0.14	0.10	0.12	0.12	0.20	0.30	0.24	0.16	0.15	0.32	0.14	0.37	0.31
Pb	<2	<2	<2	<2	<2	<2	<2	3	17	8	6	13	<2	4

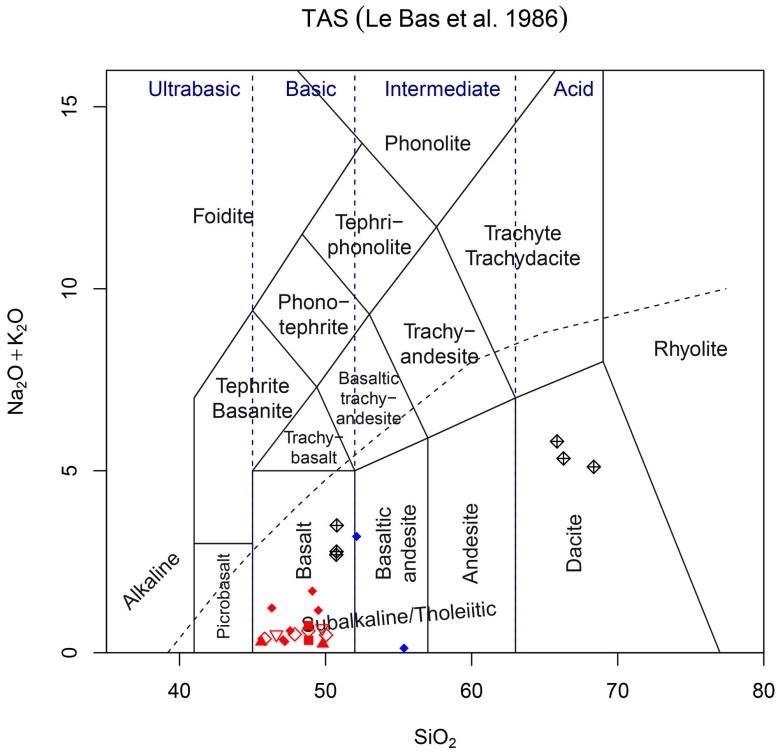

A

AFM plot (Irvine and Baragar 1971)

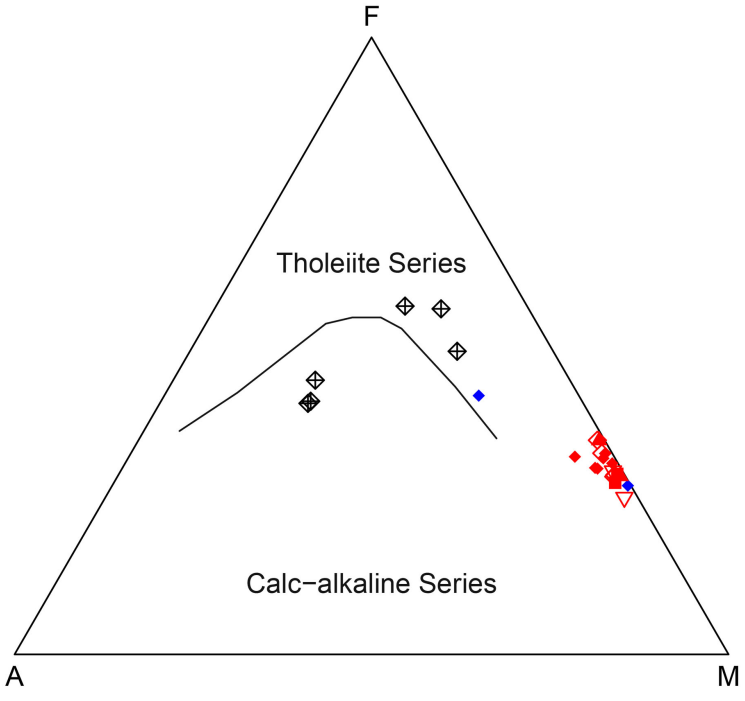

B

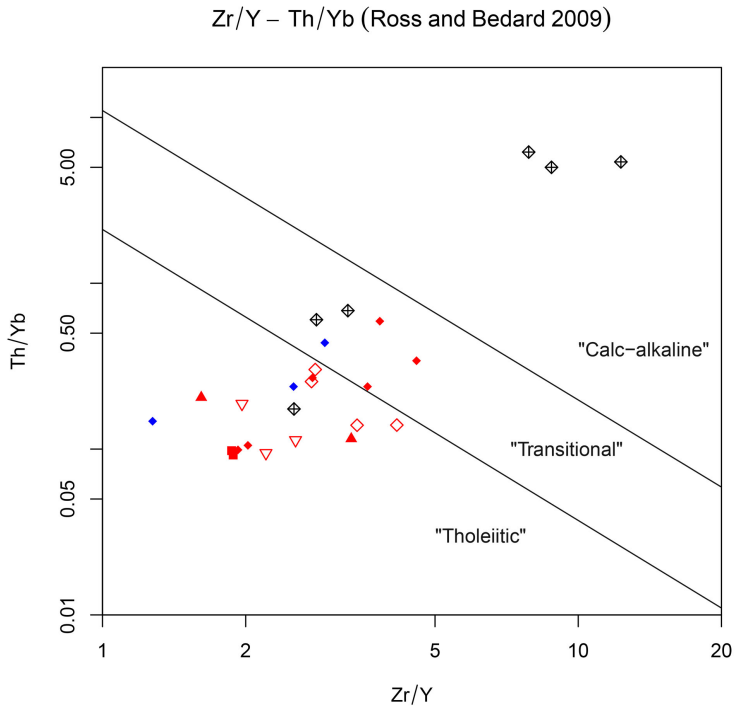

C

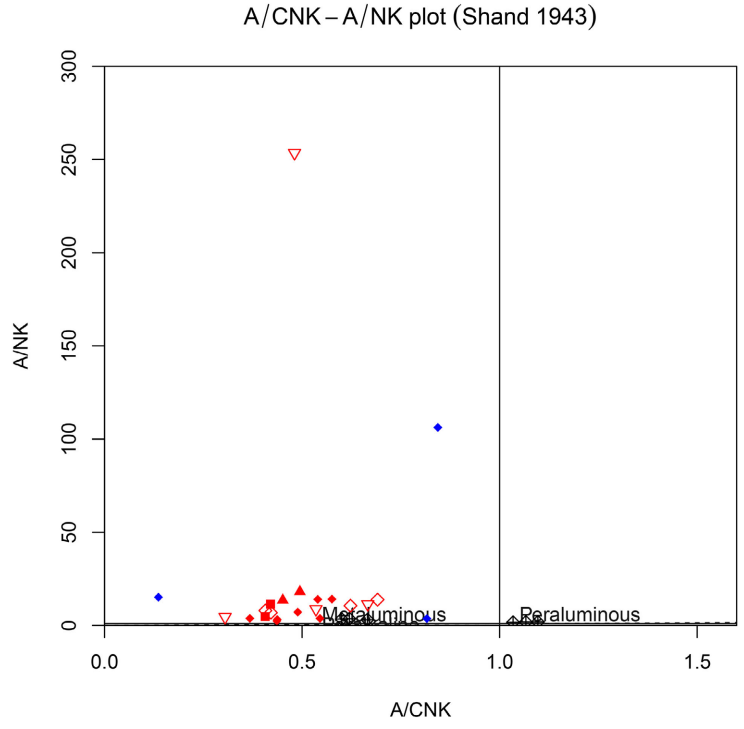

D

Figure 5. Elogo Complex metabasites' classification: A—in the discrimination diagram of TAS [11]; B, C—in the magmatic affinity discrimination diagrams respectively in [12] [13]; D—in the aluminous discrimination diagram of [14]. Red points = tholeiitic basalts; blue points = basalts and calc-alkaline andesitic basalts, black points = calc-alkaline dacites.

The samples considered tholeiitic basalts (basic and ultrabasic rocks) have a ratio of FeOt/MgO = 0.34 à 2.13, A/NK = 4.03 à 10.22 and A/CNK = 0.66 à 1.52, low alkaline contents (Na_2O + K_2O = 0.02% to 3.46%), high MgO (5.36% to 26%) and Fe_2O_3 (8.94% to 13.65%). Those attributed to basalt and calc-alkaline andesitic basalt have (FeOt/MgO = 0.35 to 0.42), A/NK = 7.39 to 22.83; A/CNK = 0.25 to 0.74 with low alkaline Na_2O + K_2O (0.12% to 0.62%) content and high CaO (7.54% to 10.95%), MgO (20.2% to 24%) and Fe_2O_3 (8.5% to 10.45%) contents. The calc-alkaline dacite samples have FeOt/MgO (1.95 to 2.23), A/NK (2.48 to 2.74), and A/CNK (1.62 to 1.70), a moderate alkaline content Na_2O + K_2O (5.11% to 5.82%) compared to basalt, a low CaO (3.05% to 3.17%), MgO (2.75% to 3.21%) and of Fe_2O_3 (5.99% to 7.27%) contents. Therefore, the Th/Yb < 0.70 and Zr/Y < 3.9 ratios place the Elogo basalts in the field of tholeiites within the Zr/Y – Th/Yb diagram of [13], where the dacites are plotted in the calc-alkaline domain (Th/Yb < 5 and Zr/Y < 7). A sample of andesitic basalt (Th/Yb = 0.43 and Zr/Y = 2.93) and two samples of dacite Th/Yb (0.60 and 0.68) and Zr/Y (2.81 and 3.27) are plotted in the transitional field between the tholeiitic series and calc-alkaline (**Figure 5(C)**). The A/NK vs. A/CNK plot diagram of [14] shows that tholeiitic basalts, basalts and calc-alkaline andesitic basalt are metaluminous and, however, calc-alkaline dacites are peraluminous (**Figure 5(D)**). Binary Harker plots of REE and trace elements contents correlated with MgO content for samples of the Elogo complex starting from tholeiitic basalts to calc-alkaline dacites (**Figure 6**). They show a positive evolution in Ni and in Cr and a negative evolution in Ba, Rb, Ce, Sr, Y, La, and Zr. Moreover, depending on the nature of the rocks, there is a varied behavior: 1) The tholeiitic basalts show an almost stable evolution for the Ba, La and Rb elements, a positive correlation for the Ni and Cr elements, a negative correlation for the Ce, Sr and Zr elements and dispersion for the Y element. 2) Basalt and andesitic basalt calc-alkalines show a negative correlation for the Ce, La, Sr, Y, and Zr elements, a positive correlation for the Ni element, a dispersion for the Cr, and a negative correlation to stable correlation for the Ba and Rb elements. 3) Dacites display a stable trend for Ni and a dispersive trend for the rest of the elements. The binary Harker diagrams of the traces elements and rare earth contents correlated this time with the Zr content show for all the rocks a positive correlation in Ba, Ce, La, Rb, Sr, Y, Nb and Ta, and a negative correlation in Ni, Co, Mg et Cr (**Figure 7**). However, depending on the rocks, the behavior varies according to the elements as in the above-mentioned: 1) The tholeiitic basalts show an almost stable evolution for the Ba, Ta, La and Rb elements, a positive correlation for the Ce element, and dispersion for the Nb, Sr, Y, Co, Cr, and Ni elements; 2) the basalts and the andesitic calc-alkaline basalts show a stable evolution for the Ta, a negative correlation for the Ni, a positive correlation for the Ba, Ce, Nb, Rb, Y, Sr, and La, a dispersion for the Co and the Cr; 3); Dacites still shows a stable trend for Ni, a negative to stable trend for the Cr and a dispersive trend for Ba, Ce, Co, La, Nb, Rb, Sr, Ta and Y.

The REE of the different rocks were normalized to the primitive mantle of [15] and a chondrite of [16] (**Figure 8(A)**, **Figure 8(B)**). The tholeiitic basalts have LREE contents (La = 0.5 ppm to 8.1ppm and Ce = 0.8 ppm to 6.6 ppm) close to and lower than those of HREE ((Yb = 0.4 ppm to 2.24 ppm and Lu = 0.05 ppm to 0.37 ppm) and according to the samples an absent to weak fractionation between LREE [(La/Yb)n = 0.36 to 0.97; (Ce/Yb)n = 0.27 to 0.96] and HREE [(La/Yb)n = 1 to 2.15; and (Ce/Yb)n = 1.04 to 1.72)], a significant negative anomaly in Eu (Eu/Eu* = 0.25 to 0.99), and which are manifested by spectra with evolution almost horizontal.

The basalts and the andesitic calc-alkaline basalts have a horizontal to sub-oblique evolution. The calc-alkaline dacites show an equally oblique evolution. Normalizations to the primitive mantle of [17] and the chondrite of [18] (**Figure 8(C)**, **Figure 8(D)**) show for the tholeiitic basalts the negative anomalies in Rb, Nb, Ba, K and Sr; and positive anomalies in Pb and Ta. The basalts and the andesitic calc-alkaline basalts show a negative anomaly in Nb and Ti and positive anomalies in Pb, Ta and U with enrichment in LILE (Cs, Th et U) and LREE (La and Ce).

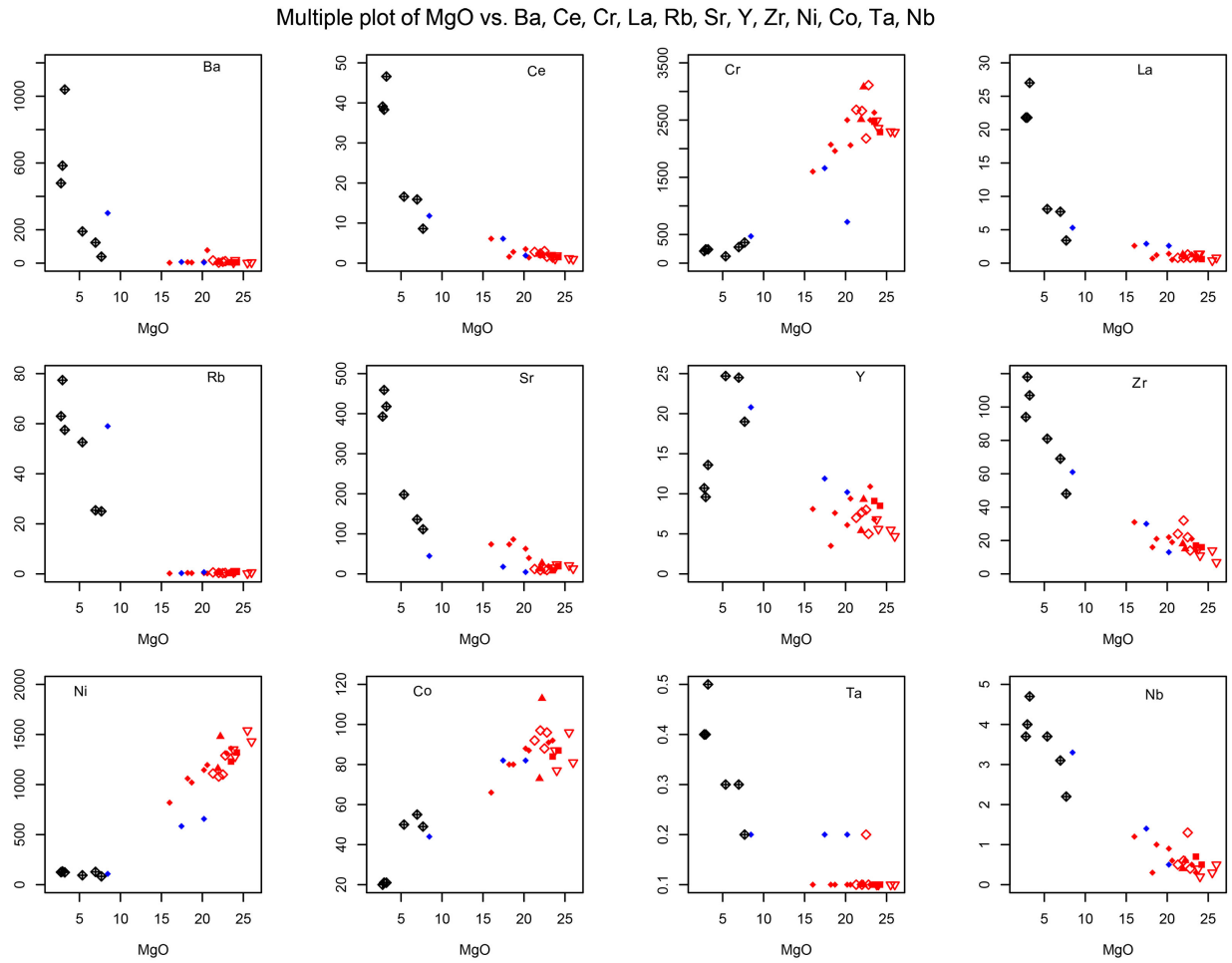

Figure 6. Binary Harker diagrams show mobile elements' evolution, REE as a function of MgO. Red points = Tholeiitic basalts; blue points = basalts and andesitic basalts, black points = calc-alkaline dacites.

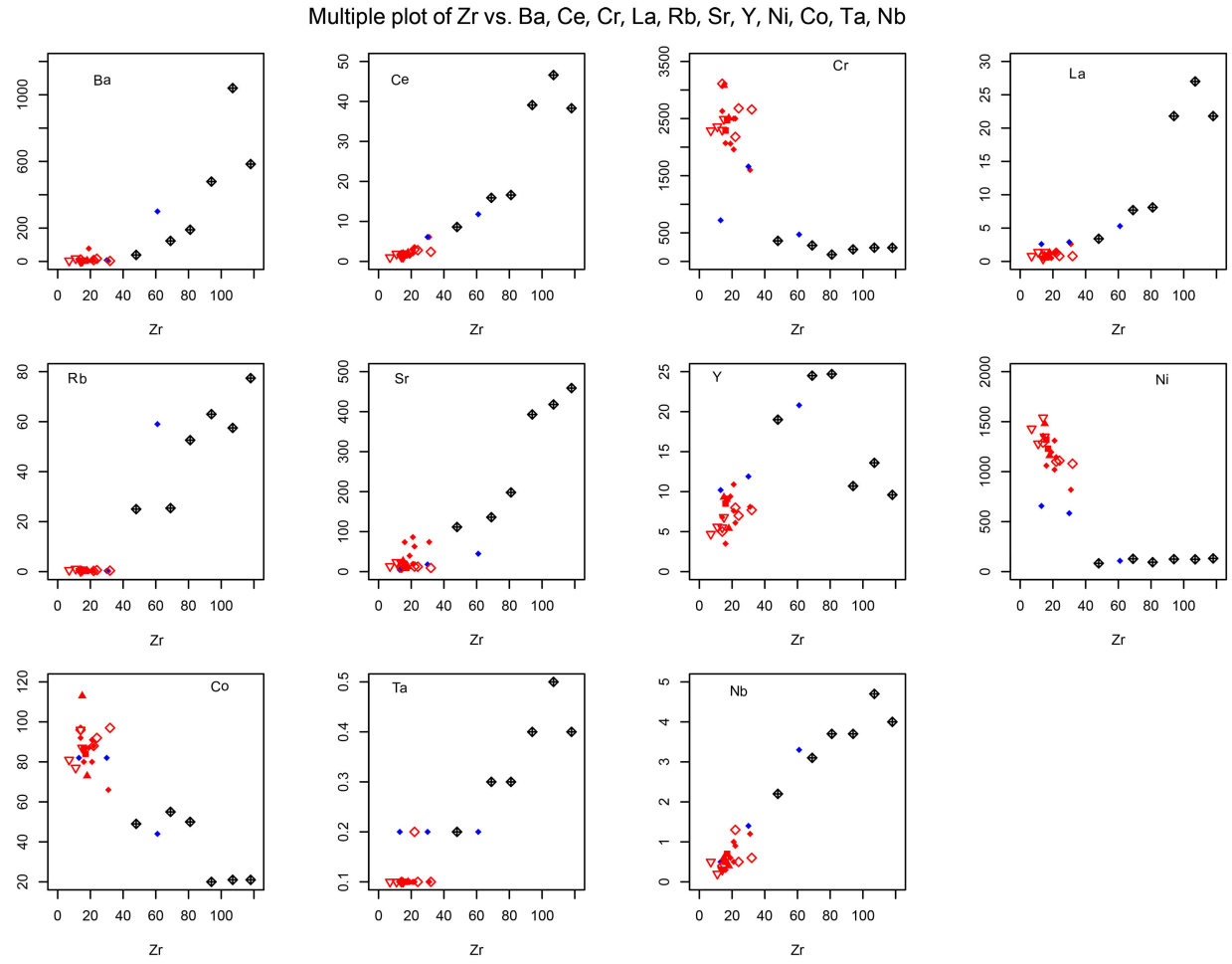

Figure 7. Binary Harker diagrams showing the evolution of mobile elements and REE as a function of Zr. Red = Tholeiitic basalts; blue = basalts and calc-alkaline andesitic basalts, black= calc-alkaline dacites.

5. Discussion

Elogo complex is one of the metamorphic units forming the greenstone belts in the Ivindo Archean Block in the Congo. It is comparable to Belinga, well studied in Gabon [4].

5.1. Petrogenesis

The metabasite rocks observed in Elogo and Bamegod are amphibolites, chlorite schists, and epidotes. The show LOI (Table 1) varied from low (0.85%) to medium (1.13% to 1.53%) and very high in most samples (16.4%). The high values testify to a post-genetic transformation linked to metamorphism or hydrothermalism. Retrograde metamorphic parageneses are marked by 1) chlorite-muscovite-talc-quartz-calcite; 2) chlorite-muscovite-cordierite-calcite-quartz-chalcopyrite; 3) epidote-actinolite-tremolite-muscovite-zoisite. Retrograde hydrothermal parageneses are characterized by relics of hornblende associated with carbonate, muscovite, and talc tremolite. Chemical analyses show that the rocks

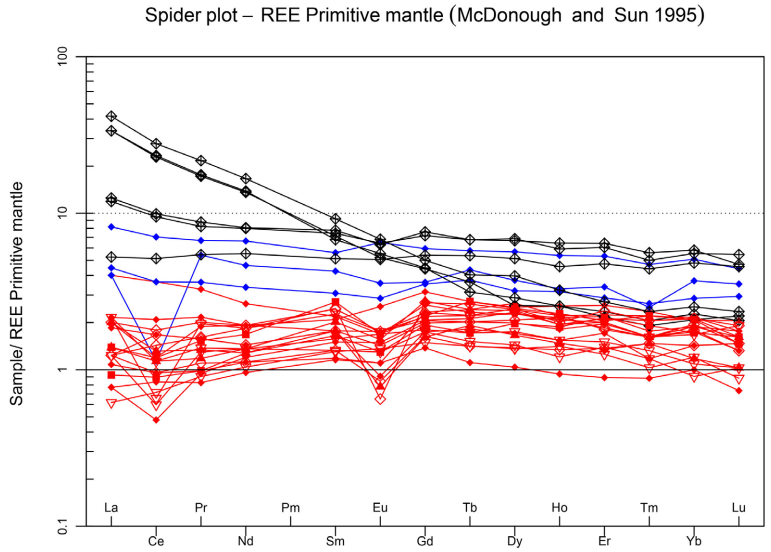
Spider plot – REE Primitive mantle (McDonough and Sun 1995)
Sample/ REE Primitive mantle
100
10
1
0.1
La
Ce
Pr
Nd
Pm
Sm
Eu
Gd
Tb
Dy
Ho
Er
Tm
Yb
Lu

A

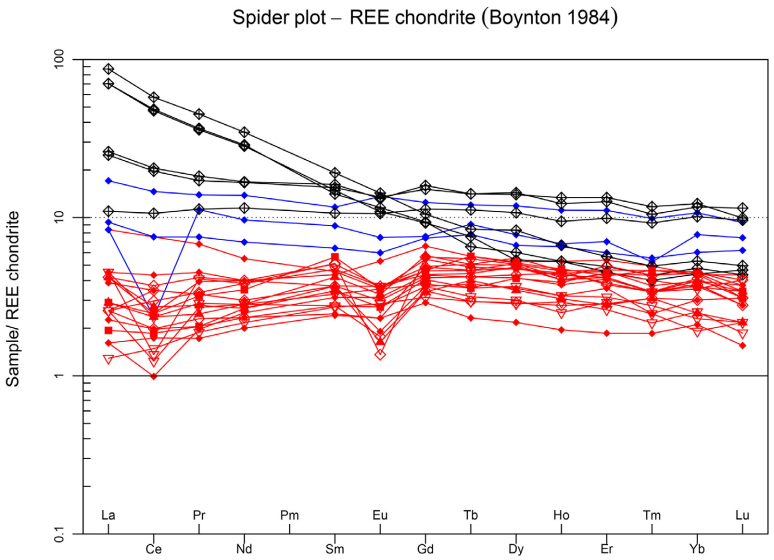
Spider plot – REE chondrite (Boynton 1984)
Sample/ REE chondrite
100
10
1
0.1
La
Ce
Pr
Nd
Pm
Sm
Eu
Gd
Tb
Dy
Ho
Er
Tm
Yb
Lu

B

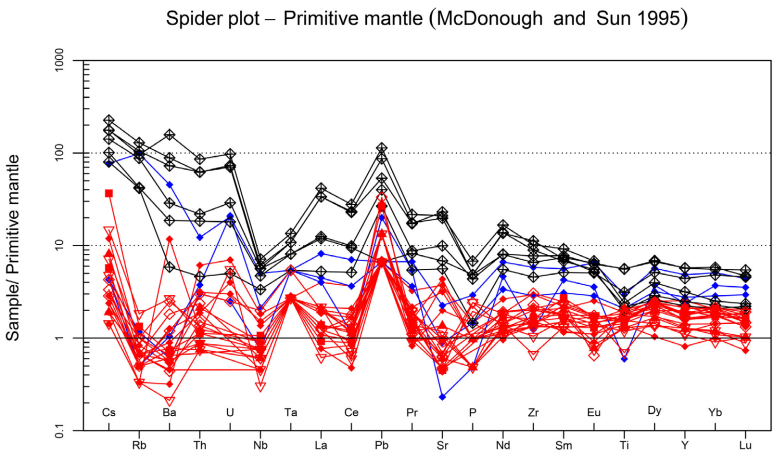
Spider plot – Primitive mantle (McDonough and Sun 1995)
Sample/ Primitive mantle
1000
100
10
1
0.1
Cs
Rb
Ba
Th
U
Nb
Ta
La
Ce
Pb
Pr
Sr
P
Nd
Zr
Sm
Eu
Ti
Dy
Y
Yb
Lu

C

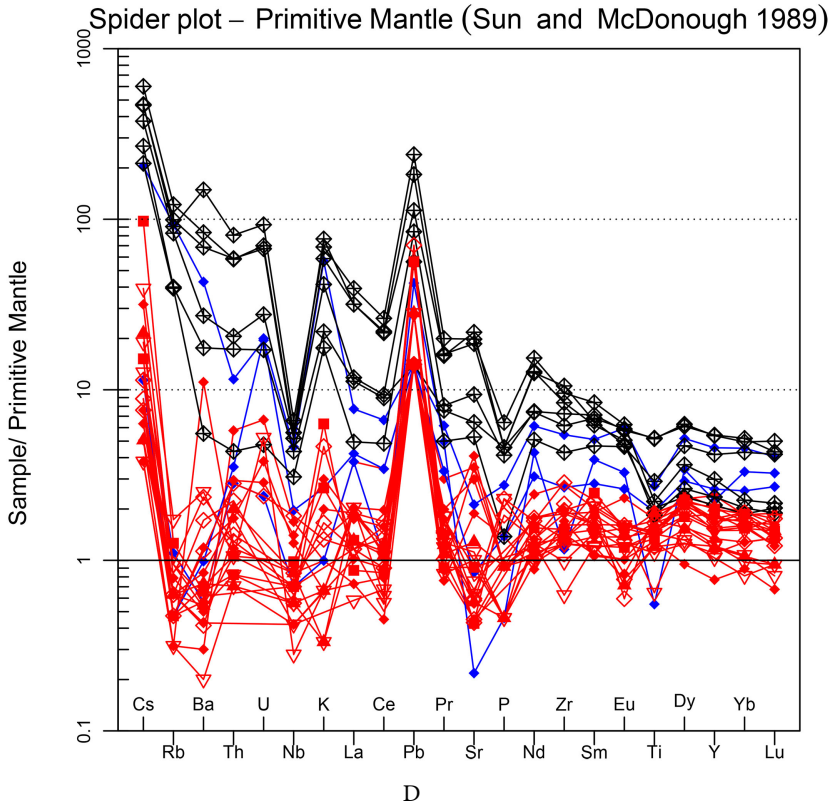

Figure 8. Diagrams of normalized REE of Elogo complex metabasites: A—to the primitive mantle of [15]; B—to the chondrite of [16]; C—Multielement diagram of traces elements normalized to the primitive mantle of [17]; D—to the chondrite of [18]. Red = Tholeiitic basalts; blue = basalts and calc-alkaline andesitic basalts; black = calc-alkaline dacites.

have undersaturated to low saturated compositions and are low TiO_2 < 2% according to [19] [20] [21] [22] [23]; these samples are classed as a rock with low Ti (TiO < 2). Major element projection diagrams (**Figure 5**) place rocks in tholeiitic basalts, basalts and calc-alkaline andesitic basalts, and calc-alkaline dacites. The tholeiitic basalts, the basalts, and calc-alkaline andesitic basalts are metaluminous, and the dacites are peraluminous. The binary Harker diagrams in trace elements and REE vs. MgO (**Figure 6**) show a positive evolution in Ni and Cr and a negative evolution in Ba, Rb, Ce, Sr, Y, La, and Zr. On the other hand, those of the trace elements and REE vs. Zr (**Figure 7**) show a positive evolution in Ba, Ce, La, Rb, Sr, Y, Nb and Ta and rather negative in Ni, respectively Co and Cr. The behavior of trace and REE elements is identical to that observed in the greenstone belts of Rio das Velhas and Pitangui greenstone belts, São Francisco Craton, Brazil [24].

5.2. Post-Genetic Alteration of Elogo Complex Metabasites

The retrograde metamorphism of amphibolite into chlorite-schists observed in the metabasites is accompanied by a significant hydrothermal circulation marked by a considerable variation in MgO contents (5.36% to 7.68%; 16% to 26%) within the basalts. The tholeiitic basalts and calc-alkaline dacites present nega-

tive anomalies in P, Rb, Ba, and Ce, and positive anomalies in Li, which symbolize this hydrothermal alteration (**Figure 8**). The retrograde metamorphism and hydrothermal alteration are considered controllers of the mobility of the LILE and REE [25] [26] [27] [28]. This mobility of the LILE continues without influencing the HFSE, HREE, Zr and Hf contents [27] [29].

Works on the mobility of chemical elements in Precambrian rocks under the effect of metamorphism as well as during hydrothermal alteration show that major elements such as Al, Ti, Fe, P and HFSE, REE, except Eu and Ce, and transition metal Cr, Ni, Sc, V, Y are relatively immobile in greenschist and amphibolites facies and even under granulite facies conditions [30]-[35]. Eoarchean metavolcanic rocks from Isua in west Greenland show that rocks with Ce/Ce* [Ce/Ce* = Cecn/(La_{cn}*Pr_{cn})1/2] < 0.9 or >1.11 exhibit REE mobility, while rocks with Ce/Ce* between 0.9 and 1.1 exhibits limited mobility of the REE [36]. Twelve (12) tholeiitic basalts samples show a strong negative Ce anomaly (**Figure 8(A)**, **Figure 8(B)**) and a weak Ce/Ce* < 0.9 ratio between 0.24 and 0.89, marking a significant mobility of the LREE linked to an important hydrothermal circulation. Calc-alkaline dacites and some tholeiitic basalts without negative Ce anomalies are marked by a Ce/Ce* ratio between 0.91 and 1.18, revealing a low LREE mobility during hydrothermal circulation. Besides, negative Eu and Sr anomalies reveal a plagioclase accumulation [37] in tholeiitic basalts (**Figure 8(A)**, **Figure 8(C)**).

5.3. Crustal Contamination in the Basalts and Dacites of Elogo Complex

Crustal contamination during the emplacement of igneous rocks can be assessed from the ratios between REE and HFSE as Nb/Yb, Th/Yb, Nb/La, La/Ta, (La/Yb)n, Y/Nb and Zr/Th known for the mantle and the continental crust [24]. The Th/Yb vs. Nb/Yb diagram that discriminates arc basalts at MORBs and OIBs, as well as crustal contamination [24] [38] [39], displays low-contaminated tholeiitic basalts and calc-alkaline basalts (Th/Yb < 0. 59) in the arc field closer to MORBs; and highly contaminated calc-alkaline dacites (Th/Yb < 0.44) in the arc field also but further from the MORB field (**Figure 9**). REE/HFSE ratios, used to assess crustal contamination, are high in the crust and low in the mantle [24]. They are higher in calc-alkaline dacites (La/Nb = 1.55 to 5.89; La/Ta = 17 to 54.5) and in calc-alkaline andesitic basalts and basalts (La/Nb = 1.66 to 5.2; La/Ta = 13 to 26) than in tholeiitic basalts (La/Nb = 0.83 to 3.5; La/Ta = 4 to 26). REE/HFSE ratios reveal more marked contamination in calc-alkaline basalts and dacites than in poorly contaminated tholeiitic basalts. Thus, REE fractionation highlights contamination in tholeiitic basalts (La/Yb)n < 1.93 (0.98 to 1.92), calc-alkaline basalts (La/Yb)n < 1.66 (0.97 to 1.65), and more significant contamination in calc-alkaline dacites (La/Yb)n > 1.93 (1.97 to 1.98). The Zr/Th ratios of the crust (Zr/Th = 20) and the mantle (Zr/Th = 116) make it possible to trace the origin and contamination of the magma; they reveal crustal contamination when they are close to the Zr/Th ratio of the crust [24] [38]. Zr/Th ratios (122.22 to 300) higher than the Zr/Th ratio of the primitive mantle indicate an absence

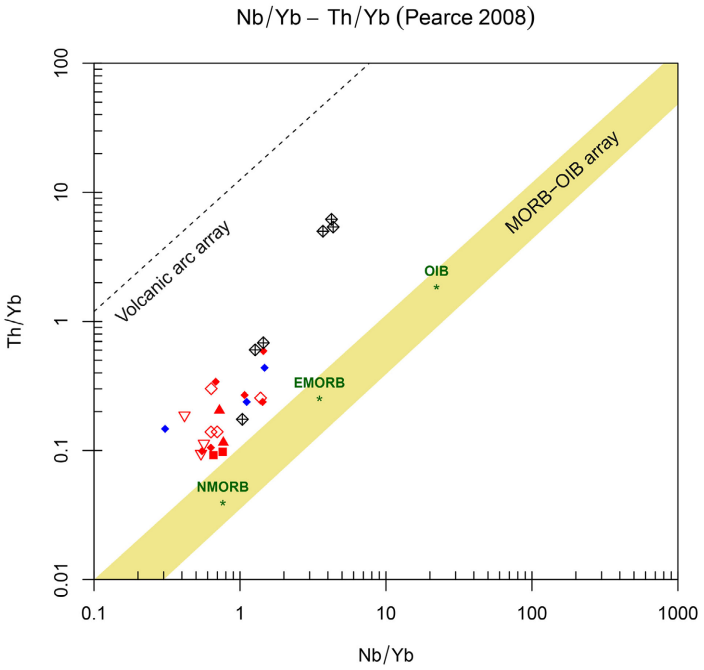

Figure 9. Geotectonic discrimination diagram of [38] using Nb/Yb vs. Th/Yb ratios to determine crustal contamination on the Elogo complex metabasite rocks. Red = tholeiitic Basalts; blue = basalts and calc-alkaline andesitic basalts, black = calc-alkaline dacites.

of contamination; on the other hand, Zr/Th ratios (63.23 - 106.66) lower than the Zr/Th ratio of the primitive mantle reveal in the tholeiitic basalts weak contamination as in the samples of calc-alkaline andesitic basalts (Zr/Th = 54.17 to 100). On the other hand, Zr/Th ratios (15.60 - 67) are lower than the mantle ratio but close to the continental crust Zr/Th ratio reveals significant contamination in the calc-alkaline dacites. Crustal contamination is also highlighted by positive Th-U-Pb anomalies in tholeiitic basalts, dacites, and calc-alkaline basalts and negative Nb-Ta anomalies in dacites (**Figure 8(C)**, **Figure 8(D)**). However, the low contamination of tholeiitic basalts and calc-alkaline andesitic basalts is also characterized by their positive Ta anomalies and low Rb-Ba contents (**Figure 8(C)**, **Figure 8(D)**).

5.4. The Composition of the Source Mantle of Basalts and Dacites of Elogo Complex

The composition of the source mantle and its depth for the rocks of the Elogo complex can be assessed by the ratios Al_2O_3/TiO_2, CaO/Al_2O_3 and $(Gb/Yb)_{PM}$ [28] [40]. Mafic and ultramafic rocks are classified as Al-depleted when $(Al_2O_{3/}TiO_2)_{adj} \leq 16$, $(CaO/Al_2O_3)_{adj} > 1.0$, and $(Gd/Yb)_{PM} > 1$ and Al-undepleted when the ratio $(Al_2O_3/TiO_2)adj > 20$, $(CaO/Al_2O_3)adj \leq 1.0$, $(Gd/Yb)_{PM} \leq 1.0$) [39] [41] [42]. The metabasites rocks of the Elogo complex (**Figure 10**) are mostly at $Al_2O_3/TiO_2 > 16$ but between 16.5 and 35.12, with however many rocks at $Al_2O_3/TiO_2 < 20$ and three tholeiitic basalts samples at $Al_2O_3/TiO_2 < 16$ (12.45

to 14.48). The ratio CaO/Al_2O_3 is <1 in twelve tholeiitic basalt samples (0.52 à 0.97) and the calc-alkaline dacites (0.21 to 0.23). This ratio is >1 in ten samples of tholeiitic basalt (1.04 to 1.35) and basalts and calc-alkaline andesitic basalts (1.28, 1.68 and 3.99). The ratio $(Gd/Yb)_{PM} > 1$, except for two basalt samples which have a ratio $(Gb/Yb)_{PM} < 1$ (0.97 and 0.98). The Al_2O_3/TiO_2, CaO/Al_2O_3 and $(Gb/Yb)_{PM}$ ratios show that part of the mantle is of the undepleted type and may contain garnet in the melting (deep source) and another part is of the depleted type (shallow source). The Th, Nb, Zr and Hf are used to determine the quality of the mantle source for the magma. The positive anomalies in Th and the flat evolution of Zr, Hf and Ti observed in the tholeiitic basalts indicate an undepleted mantle. The negative Th, Nb, Zr, and Hf anomalies reflect an origin linked to the depleted mantle in the tholeiitic basalts, calc-alkaline basalts, and calc-alkaline dacites [43]. The high MgO content helps identify melting temperatures [44] [45]. Tholeiitic basalt and calc-alkaline andesitic basalts with MgO between 16% and 26% characterize very high melting temperatures located

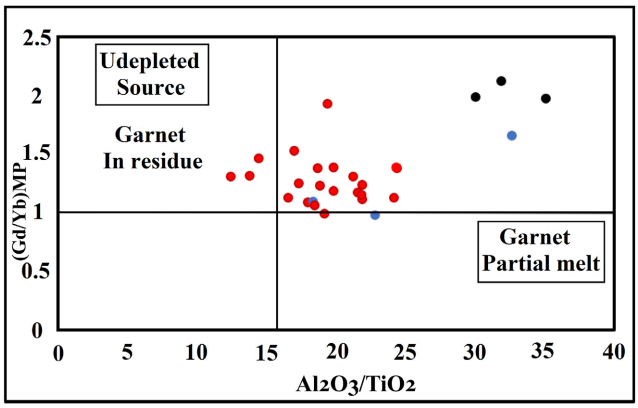

A

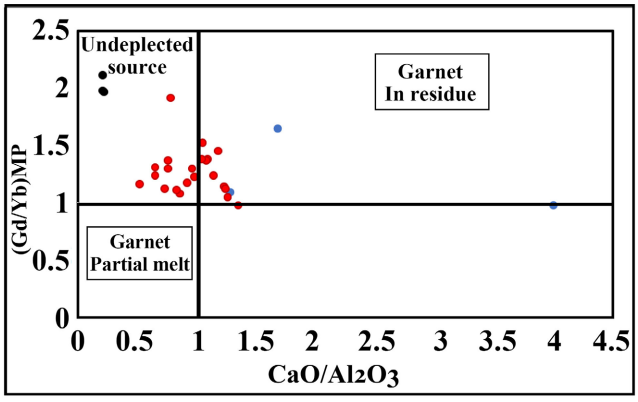

B

Figure 10. The plot of metabasite rocks of Elogo complex in diagrams of [42] modified by [9]: A - Al_2O_3/TiO_2 vs. $(Gb/Yb)_{PM}$; B - CaO/Al_2O_3 vs. $(Gb/Yb)_{PM}$. Tholeiitic basalts and dacites fall in undepleted source, and some tholeiitic basalts samples and three calc-alkaline andesitic basalts samples are in the garnet residue domain. Red = tholeiitic basalts; bleu = basalts and calc-alkaline andesitic basalts; black = calc-alkaline dacites.

from 1484, 09˚C to 1681, 77˚C and calc-alkaline dacites with contents between 2.75% and 3.21% showed low melting temperature located between 434.76˚C and 592.99˚C. Therefore, melting temperatures are calculated by [Tp(˚c) = 1463 + 12.74MgO − 2924/MgO] formula of [45].

5.5. Geodynamic Context of Metabasite Elogo Complex

Most studied metabasites are characterized by negative Rb, Ba, Nb, Sr, and Eu anomalies. On the other hand, a few samples show positive anomalies in Ta and Sr, negative anomalies in Rb and Ba, and positive in Ta in the tholeiitic basalts and andesitic basalts calc-alkalines characterize an extensive tectonic context exempt from significant crustal contamination. Nb/Yb vs. Th/Yb diagram of [38] (**Figure 9**) plot samples in NMORB, EMORB and volcanic arc array. La/Yb vs. Nb/La diagram of [46] (**Figure 11(A)**) plots tholeiitic basalts in MORB and oceanic arcs domains, with one sample in a continental arc. The tholeiitic basalts and calc-alkaline andesitic basalts are located in the continental and oceanic arc domains. The dacites are situated in MORB, continental and alkaline arcs. The La/Yb vs. Th/Nb diagram of [46] (**Figure 11(B)**), on its side, places the tholeiitic basalts largely in oceanic arc domains with some samples in continental arcs field. The basalts and calc-alkaline andesitic basalts are plotted in continental and oceanic arc fields, and dacites are in alkaline continental and oceanic arc fields. All the projections show that the tholeiitic basalts have an oceanic character with an influence of arc domains, particularly the oceanic arc domain. These rocks' anomalous negative in Nb and positive in Ta and free from a negative anomaly in Ti exclude the subduction context for their geodynamic context.

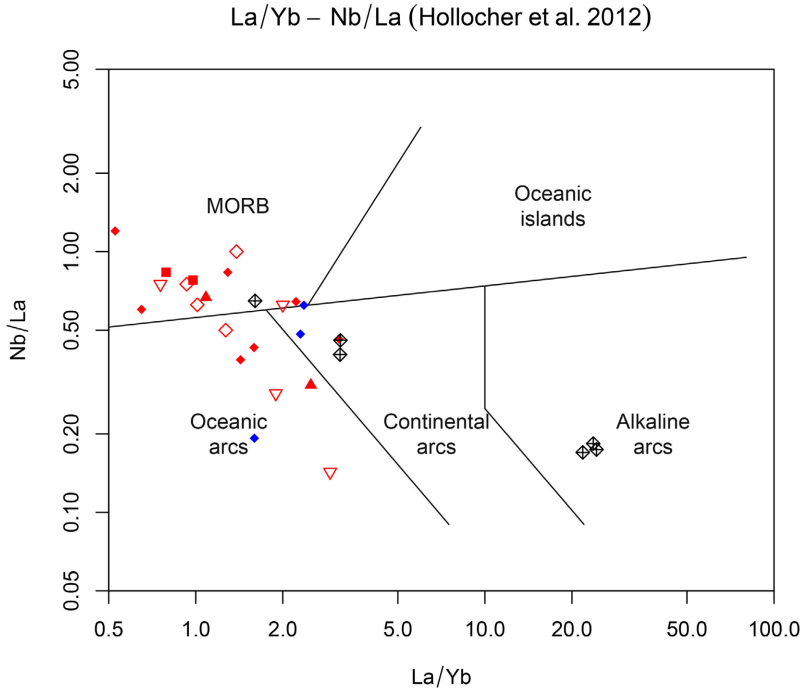

A

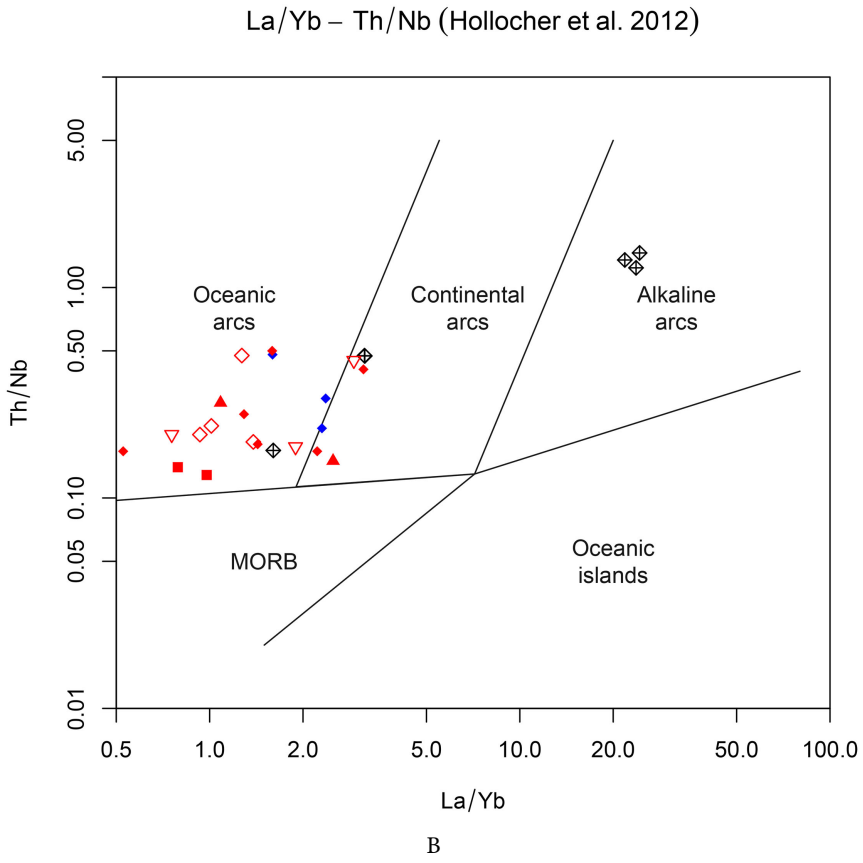

Figure 11. Geotectonic discrimination diagrams of [46] applied to metabasites of Elogo complex. A—La/Yb vs Nb/La; B—La/Yb vs Th/Nb. Red = tholeiitic basalts; blue = basalts and calc-alkaline andesitic basalts; black = calc-alkaline dacites.

The positive Pb anomaly and the weak LREE depletion with a ratio $(La/Yb)_{PM}$ ~ 1 are geochemical signatures excluding a mid-ocean ridge tectonic context with a well-elaborated oceanic crust, but relatively favorable to an extensive continental rift-type tectonic context with a beginning of oceanization or a back-arc basin type tectonic context. The high ratios Nb/Th (2 to 10), Nb/U (1.82 to 26) and La/Ta (5 to 27) of tholeiitic basalts are characteristic of sources and /or remnants of divergent margin magmatism [47]. The diagram Nb/Yb vs. Th/Yb of [38] (**Figure 9**) plots calc-alkaline dacites in the contaminated volcanic back-arc domain. As for La/Yb vs. Nb/La and La/Yb vs. Th/Nb of diagrams of [46] (**Figure 11**), the basalts are in the domain of alkaline arcs and continental arcs. The association of the signature of NMORBs and island-arc basalts (**Figure 11**) within the basalts reveals a back-arc basin context [48]-[53]. Thus, the tholeiitic basalts of the Elogo complex were formed following an extensive geodynamic regime of the back-arc basin type. FeOT-MgO-Al_2O_3 triangular diagram of [54] (**Figure 12(A)**) plots all kinds of basalts in ocean ridge and floor and scatters dacites in four domains (orogenic, ocean Island, continental, ocean ridge and floor). The calc-alkaline andesitic basalts and dacites are not like the tholeiitic basalts in the domain of the ridge and the ocean floor but rather in the orogenic

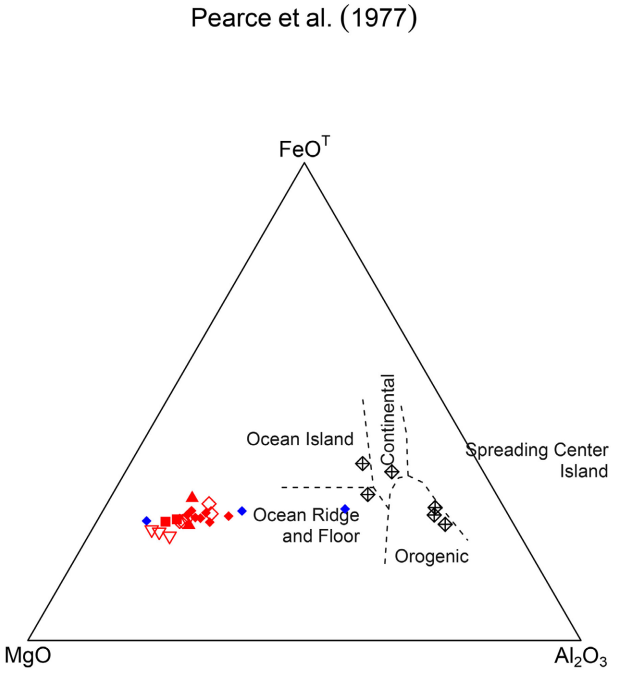

A

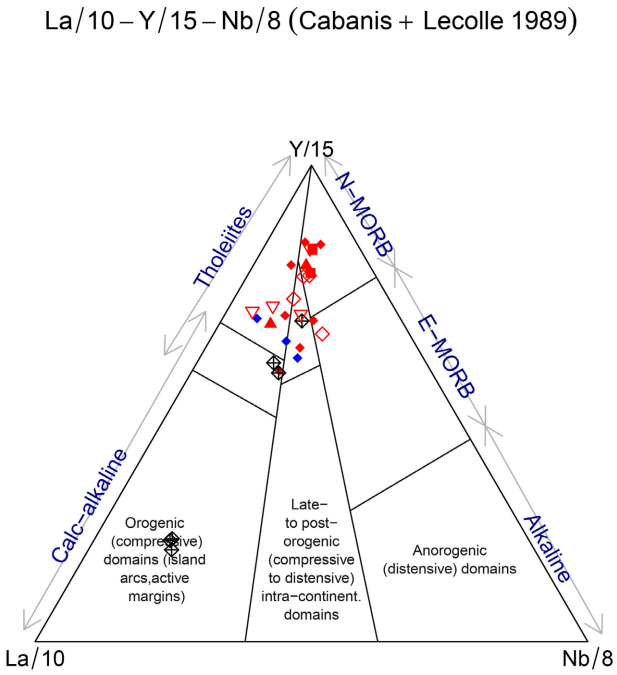

B

Figure 12. A—Geotectonic discrimination of metabasite Elogo complex in MgO-Al_2O_3-FeOT triangular diagram of [54]: All basalts are in ocean Ridge and Floor. Dacites are distributed in all domains. B—Basalts and dacites discrimination in the MORB field, compressive arc, and intracontinental rift field, according to [55]. MORB = Mid-Ocean Ridge Basalts, CRB = Continental Rift Basalts, IAB = Island Arc Basalts, OIB = Ocean Island Basalts, and BAB = Back arc basalts. The area circled in green in diagram B corresponds to the back-arc basins (BAB). Sample Red = tholeiitic basalts; bleu = basalts and calc-alkaline andesitic basalts; black = calc-alkaline dacites.

and continental domains. Indeed, in the ternary diagram of the ratios of trace elements and REE La/10, Y/15 and Nb/8 (**Figure 12(B)**) of [55], the tholeiitic basalts of the Elogo complex are plotted in the rear basin oceanic arc field and at the transition between the BAB and N-MORB domain mainly (**Figure 12(B)**). Similarly, the signature of the calc-alkaline andesitic basalts and the dacites (positive anomalies in U, Th, K, Li, La, Pb, Ce and negatives anomalies in Nb and Ti) reflects crustal contamination and hydrothermal alteration as observed in thin sections. The geochemical signature of calc-alkaline andesitic basalts and dacites is characteristic of a compressive tectonic context affecting the back-arc basin in which the tholeiitic basalts were previously emplaced. The metabasites characterize two main tectonic phases: 1) a first extensive phase at the back-arc inducing a basin in which take place the tholeiitic basalts of intermediate type between NMORB and EMORB; 2) a second tectono-metamorphic phase compressing the basin; it would be associated with subduction accompanied by hydrothermal circulations.

The tholeiitic basalts (basic and ultrabasic rocks), except for a few samples, are comparable in MgO (16% to 26%), Al_2O_3 (4.7% to 15%), Co (44 to 113 ppm), Cr (1600 ppm to 3110 ppm) and in Ni (1060 ppm to 1540 ppm) to the basic-ultrabasic rocks to Belinga greenstone belt of Gabon [4]. In this last country, the greenstone belt is considered to have been emplaced during the Meso-Neoarchean extension (between 2870 Ma and 2750 Ma, the age of reworked zircons and the tectonometamorphic event that affects the greenstone of Belinga group). Calc-alkaline andesitic basalts and dacites, which present a geochemical signature of a compressive tectonic regime, closure of a back-arc basin by possible subduction would be related to this tectono-metamorphic event of [4]. Similarly, the relics of the greenstone belts of the Ntem complex in Cameroun, particularly the greenstone belt of Lolodof-Ngomezap dated to Mesoarchean (around 3000 Ma) by [56], present a tholeiitic and calc-alkaline affinity like the basalts and dacites of Elogo.

6. Conclusions

Elogo complex's amphibolites are related to tholeiitic basalts (SiO_2 = 37.4 to 50.7%; FeOt/MgO = 0.34 to 2.13) metaluminous (A/NK = 4.03 to 102.22 and A/CNK = 0.66 to 1.52); chlorite schists and epidote rock are similar to calc-alkaline basalts and andesitic basalts (SiO_2 = 46.1% to 47.4% and 53.1%; FeOt/MgO = 0.35 to 0.42 and 0.38 respectively) metaluminous (A/NK = 7.39 to 12.78 and 22.83; A/CNK = 0.55 to 0.74 and 0.25 respectively). Gneissic amphibolites are similar to calc-alkaline dacites (SiO_2 = 65.2% to 66%; FeOt/MgO = 1.95 to 2.23) hyperaluminous (A/NK = 2.48 to 2.74 and A/CNK = 1.62 to 1.70). Trace element geochemistry of basalts and dacites reveals that:

- The retrograde chlorite-calcite-muscovite-talc-hematite paragenesis, negative Rb, Ba, Ce ($Ce/Ce^* < 0.7$) and P anomalies, and positive Li anomalies in the basalts are typical of hydrothermal alteration.

- The low contamination of calc-alkaline tholeiitic and andesitic basalts is emphasized by a Th/Yb < 1 ratio, a positive Ta anomaly, and by low Rb-Ba contents compared to highly contaminated (Th/Yb > 1) and fractionated calc-alkaline dacites [(La/Yb)n > 1. 93] with high La/Nb (1.5 to 5.85) and La/Ta (17 to 54.5) ratios, Zr/Th (15.598 to 67) close to continental crust (Zr/Th = 20) and positive Th-U-Pb and negative Nb-Ta anomalies.
- The tholeiitic basalts have a depleted mantle source, including garnet in the melt residue [Al_2O_3/TiO_2 = 12.45 to 14.48 and >16 (16.5 to 32.71); CaO/Al_2O_3 < 1 (0. 52 to 0.97) and >1 (1.04 to 1.35) and $(Gb/Yb)_{PM}$ > 1] whereas dacites have a shallow source in the spinel field [Al_2O_3/TiO_2 > 16; CaO/Al_2O_3 < 1 and $(Gb/Yb)_{PM}$ > 1].
- The high MgO content in tholeiitic basalts (16% - 26%), in calc-alkaline basalts (20.2% - 24%), and low in calc-alkaline dacites (2.75% - 3.21%) mark very high melting temperatures of 1484.09˚c - 1681.778˚c and 1575.6˚c - 1646.9˚c, and low of 434.76˚c - 592.99˚c respectively. The difference in temperature and melting degree within basalts and between basalts and dacites characterize the variation in the depth of the depleted mantle source. Thus, the negative Th, Nb, Zr, and Hf anomalies of calc-alkaline basalts characterize a depleted mantle source, supported by the negative Th, Nb, and Zr anomalies of calc-alkaline dacites.
- The genesis of the basalts is explained by an extensive context that did not reach the MORB stage, justifying the positive Ta, negative Rb, Ba, and Nb anomalies associated with the lack of a negative Ti anomaly. A back-arc extension would explain well in the tholeiitic basalts the positive Ta and Li anomaly, the low Ti grades, the negative Rb and Ba anomalies, the horizontal evolution of the REE (La/Yb ~1) and the low grades in Zr and Hf.
- The geochemical signature of calc-alkaline andesitic basalts and dacites would be typical of a volcanic arc context in a subduction regime characterized by an enrichment in LILE and LREE defined by positive anomalies in Ba, U, Th, K, La, and Ce; and by a depletion in HFSE revealed by negative anomalies in Nb, Ta, and Ti.

The geochemical study reveals a back-arc extension inducing the genesis of poorly contaminated tholeiitic basalts, the extension of the complex was associated with the Meso-Neoarchean distension controlling the genesis of the Belinga group in Gabon and that of the relics of the Ntem complex rock belts in Cameroon. The distension is interrupted by the closure of the back-arc basin inducing the formation of calc-alkaline dacites and basalts in a subduction regime associated with the tectono-metamorphic event of the Belinga Group.

Acknowledgements

We thank MAC Congo for funding the field research and all the laboratory analyses. We also thank our research structure, the National Institute for Research in Exact and Natural Sciences (IRSEN) of Congo.

Conflicts of Interest

The authors declare no conflicts of interest regarding the publication of this paper.

References

[1] Thiéblemont, D., Liégeois, J.P., Fernandez-Alonso, M., Ouabadi, A., Le Gall, B., Maury, R., Jalludin, M., Vidal, M., Ouattara-Gbélé, C., Tchaméni, R., Michard, A., Nehlig, P., Rossi, P. and Chêne, F. (2016) Geological Map of Africa at 1:10 M Scale. Editors CGMW-BRGM, Orléans.

[2] Gourcerol, B., Blein, O., Chevillard, M., Callec, Y., Boudzoumou, F. and Djama, L.M.J. (2022) Depositional Setting of Archean BIFs from Congo: New Insight into under-Investigated Occurrences. *Minerals*, **12**, Article No. 114. https://doi.org/10.3390/min12020114

[3] Tchameni, R., Mezger, K., Nsifa, N.E. and Pouclet, A. (2001) Crustal Origin of Early Proterozoic Syenites in the Congo Craton (Ntem Complex), South Cameroon. *Lithos*, **57**, 23-42. https://doi.org/10.1016/S0024-4937(00)00072-4

[4] Thiéblemont, D., Castaing, C., Billa, M., Bouton, P. and Preat, A. (2009) Notice explicative de la Carte géologique et des Ressources minérales de la République gabonaise à 1/1 000 000. Editions DGMG-Ministère des Mines, du Pétrole, des Hydrocarbures, Libreville, 381 p.

[5] Gatsé Ebotouhena, C., Xie, Y., Adomako-Ansah, K. and Qu, Y. (2021) Petrology, Geochronology and Zircon U-Pb-Lu-Hf Isotopes of Granitoids from the Ivindo Basement Complex of the Souanké Area, Republic of Congo: Insights into the Evolution of Archean Continental Crust. *Geological Journal*, **56**, 4861-4887. https://doi.org/10.1002/gj.4219

[6] Loemba R.P.A., Ntsiele L.J.E.P., OPO F., Bazebizonza N., Nkodia H.M.D.V. and Boudzoumou F. (2022) Crustal Growth of Archean and Early Proterozoic Granitoids of the Ivindo Region in the Souanké and Bomalinga Areas from Central Congo Craton (North-West Republic of Congo). EGU General Assembly, Vienne. https://doi.org/10.5194/egusphere-egu22-5438

[7] Abbott, D., Burgess, L., Longhi, J. and Smith, W.H.F. (1994) An Empirical Thermal History of the Earth's Upper Mantle. *Journal of Geophysical Research*: *Solid Earth*, **99**, 13835-13850. https://doi.org/10.1029/94JB00112

[8] Herzberg, C. and O'Hara, M.J. (1998) Phase Equilibrium Constraints on the Origin of Basalts, Picrites, and Komatiites. *Earth-Science Reviews*, **44**, 39-79. https://doi.org/10.1016/S0012-8252(98)00021-X

[9] Arndt, N.T., Lesher, C.M. and Barnes, S.J. (2008) Komatiites: New York. Cambridge University Press, Cambridge, 467 p.

[10] Kessi, C. (1992) Le socle archéen et les formations ferrifères du Chaillu au Congo. Université de Rennes, Rennes.

[11] Le Bas M.J., Le Maitre R.W., Streckeisen A. and Zanettin B. (1986) A Chemical Classification of Igneous Rocks Based on the Total Alkali-Silica Diagram. *Journal of Petrology*, **27**, 775-750. https://doi.org/10.1093/petrology/27.3.745

[12] Irvine, T.N. and Baragar, W.R.A. (1971) A Guide to Chemical Classification of the Common Volcanic Rocks. *Canadian Journal of Earth Science*, **8**, 523-548. https://doi.org/10.1139/e71-055

[13] Ross, P.S. and Bédard, J.H. (2009) Magmatic Affinity of Modern and Ancient Subalkaline Volcanic Rocks Determined from Trace-Element Discriminant Diagrams.

Canadian Journal of Earth Sciences, **46**, 823-839. https://doi.org/10.1139/E09-054

[14] Shand, S.J. (1943) Eruptive Rocks. Their Genesis, Composition, Classification, and Their Relation to Ore-Deposits with a Chapter on Meteorite. John Wiley and Son, New York.

[15] McDonough, W.F. and Sun, S.S. (1995) The Composition of the Earth. *Chemical Geology*, **120**, 223-253. https://doi.org/10.1016/0009-2541(94)00140-4

[16] Boynton, W.V. (1984) Geochemistry of the Rare Earth Elements: Meteorite Studies. In: Henderson, P., Ed., *Rare Earth Element Geochemistry*, Elsevier, Amsterdam, 63-114. https://doi.org/10.1016/B978-0-444-42148-7.50008-3

[17] Sun, S.S. and McDonough, W.F. (1989) Chemical and Isotopic Systematics of Oceanic Basalts: Implications for Mantle Composition and Processes. *Geological Society, London, Special Publications*, **42**, 313-345. https://doi.org/10.1144/GSL.SP.1989.042.01.19

[18] Thompson, R.N. (1982) Magmatism of the British Tertiary Volcanic Province. *Scottish Journal of Geology*, **18**, 49-107. https://doi.org/10.1144/sjg18010049

[19] Bellieni, G., Comin-Chiaramonti, P., Marques, L.S., Melfi, A.J., Piccirillo, E.M., Nardy, A.J.R. and Roisenberg, A. (1984) High and Low-TiO_2 Flood Basalts from the Parana Plateau (Brazil): Petrology and Geochemical Aspects Bearing on Their Mantle origin. *Neues Jahrbuch für Mineralogie* (*Abhandlungen*), **150**, 273-306.

[20] Bellieni, G., Brotzu, P., Comin-Chiaramonti, P., Ernesto, M., Melfi, A., Pacca, I.G. and Piccirillo, E.M. (1984) Flood Basalt to Rhyolite Suites in the Southern Paraná Plateau (Brazil): Palaeomagnetism, Petrogenesis and Geodynamic Implications. *Journal of Petrology*, **25**, 579-618. https://doi.org/10.1093/petrology/25.3.579

[21] Piccirillo, E.M., Comin-Chiaramonti, P., Melfi, A.J., Stolfa. D., Bellieni, G., Marques, L.S., Giaretta, A., Nardy, A.J.R., Pinese, J.P.P., Raposo, M.I.B. and Roisenberg, A. (1988) Petrochemistry of Continental Flood Basalt-Rhyolite Suites and Related Intrusives from the Bassin du Paraná (Brésil). In: Piccirillo, E.M. and Melfi, A.J., Eds., *The Mesozoic Flood Volcanism of the Parana Basin*: *Petrogenetic and Geophysical Aspects*, Instituto Astronomica e Geofisico Publishers, IAG-USP Press, Sao Paulo, 107-156.

[22] Peate, D.W., Hawkesworth, C.J. and Mantovani, M.S.M. (1992) Chemical Stratigraphy of the Paraná Lavas (South America): Classification of Magma Types and Their Spatial Distribution. *Bulletin of Volcanology*, **55**, 119-139. https://doi.org/10.1007/BF00301125

[23] Peate, D.W., Hawkesworth, C.J., Mantovani, M.S.M., Rogers, N.W. and Turner, S.P. (1999) Petrogenesis and Stratigraphy of the High-Ti/Y Urubici Magma Type in the Paraná Flood Basalt Province and Implications for the Nature of 'Dupal'-Type Mantle in the South Atlantic Region. *Journal of Petrology*, **40**, 451-473. https://doi.org/10.1093/petroj/40.3.451

[24] Verma, S.K., Oliveira, E.P., Silva, P.M., Moreno, J.A. and Amaral, W.S. (2017) Geochemistry of Komatiites and Basalts from the Rio das Velhas and Pitangui Greenstone Belts, São Francisco Craton, Brazil: Implications for the Origin, Evolution, and Tectonic Setting. *Lithos*, **284-285**, 560-577. https://doi.org/10.1016/j.lithos.2017.04.024

[25] Arndt, N.T., Teixeira, N.A. and White, W.M. (1989) Bizarre Geochemistry of Komatiites from the Crixás Greenstone Belt, Brazil. *Contributions to Mineralogy and Petrology*, **101**, 187-197. https://doi.org/10.1007/BF00375305

[26] Gruau, G., Tourpin, S., Fourcade, S. and Blais, S. (1992) Loss of Isotopic (Nd, O) and Chemical (REE) Memory during Metamorphism of Komatiites: New Evidence

from Eastern Finland. *Contributions to Mineralogy and Petrology*, **112**, 66-82. https://doi.org/10.1007/BF00310956

[27] Lesher, C.M. and Stone, W.E. (1996) Exploration Geochemistry of Komatiites. In: Wyman, D.A., Ed., *Igneous Trace Element Geochemistry*: *Applications for Massive Sulphide Exploration*. *Short Course*, 12, Geological Association of Canada, St. John's, 153-204.

[28] Chavagnac, V. (2004) A Geochemical and Nd Isotopic Study of Barberton Komatiites (South Africa): Implication for the Archean Mantle. *Lithos*, **75**, 253-281. https://doi.org/10.1016/j.lithos.2004.03.001

[29] Arndt, N.T. (1986) Differentiation of Komatiite Flows. *Journal of Petrology*, **27**, 279-301. https://doi.org/10.1093/petrology/27.2.279

[30] Humphris, S.E. and Thompson, G. (1978) Trace Element Mobility during Hydrothermal Alteration of Oceanic Basalts. *Geochimica et Cosmochimica Acta*, **42**, 127-136. https://doi.org/10.1016/0016-7037(78)90222-3

[31] Ludden, J.N. and Gelinas, L. (1982) Trace Element Characteristics of Komatiites and Komatiitic Basalts from the Abitibi Metavolcanic Belt of Quebec. In: Arndt, N.T. and Nisbet, E., Eds., *Komatiites*, George Allen and Unwin, London, 331-346.

[32] Arndt, N.T. (1994) Archaean Komatiites. In: Condie, K.C., Ed., *Archaean Crustal Evolution*, Elsevier, Amsterdam, 11-44. https://doi.org/10.1016/S0166-2635(08)70219-6

[33] Polat, A. and Hofmann, A.W. (2003) Alteration and Geochemical Patterns in the 3.7-3.8 Ga Isua Greenstone Belt, West Greenland. *Precambrian Research*, **126**, 197-218. https://doi.org/10.1016/S0301-9268(03)00095-0

[34] Manikyamba, C., Kerrich, R., Khanna, T.C., Satyanarayanan, M. and Keshav Krishna, A. (2009) Enriched and Depleted Arc Basalts, with Mg-Andesites and Adakites. A Potential Paired Arc-Back-Arc of the 2.6 Ga Hutti Greenstone Terrane, India. *Geochimica et Cosmochimica Acta*, **73**, 1711-1736. https://doi.org/10.1016/j.gca.2008.12.020

[35] Manikyamba, C., Santosh, M., Chandan Kumar, B., Rambabu, S., Li, T., Saha, A., Khelen, A.C., Ganguly, S., Singh, T.D. and Subba Rao, D.V. (2016) Zircon U-Pb Geochronology, Lu-Hf Isotope Systematics, and Geochemistry of Bimodal Volcanic Rocks and Associated Granitoids from Kotri Belt, Central India: Implications for Neoarchean-Paleoproterozoic Crustal Growth. *Gondwana Research*, **38**, 313-333. https://doi.org/10.1016/j.gr.2015.12.008

[36] Kumar, N., Mann, S., Rana, S., Kumari, S., Yashpal and Ashwani, P. (2022) Geochemistry of the Neoproterozoic Volcanic Rocks of the Nakora Area of Malani Igneous Suite, Barmer District, Western Rajasthan, India. *Open Journal of Geology*, **12**, 91-110. https://doi.org/10.4236/ojg.2022.122005.

[37] Polat, A., Hofmann, A.W. and Rosing, M.T. (2002) Boninite-Like Volcanic Rocks in the 3.7-3.8 Ga Isua Greenstone Belt, West Greenland: Geochemical Evidence for Intra-Oceanic Subduction Zone Processes in the Early Earth. *Chemical Geology*, **184**, 231-254. https://doi.org/10.1016/S0009-2541(01)00363-1

[38] Pearce, J.A. (2008) Geochemical Fingerprinting of Oceanic Basalts with Applications to Ophiolite Classification and the Search for Archean Oceanic Crust. *Lithos*, **100**, 14-48. https://doi.org/10.1016/j.lithos.2007.06.016

[39] Fan, J. and Kerrich, R. (1997) Geochemical Characteristics of Aluminium Depleted and Undepleted Komatiites and HFSE-Enriched Low-Ti Tholeiites, Western Abitibi Greenstone Belt: A Heterogeneous Mantle Plume-Convergent Margin Environment. *Geochimica et Cosmochimica Acta*, **61**, 4723-4744.

https://doi.org/10.1016/S0016-7037(97)00269-X

[40] Jahn, B.M., Gruau, G. and Glikson, A.Y. (1982) Komatiites of the Onverwacht Group, South Africa: REE Geochemistry, Sm/Nd Age and Mantle Evolution. *Contributions to Mineralogy and Petrology*, **80**, 25-40. https://doi.org/10.1007/BF00376732

[41] Arndt, N.T. and Nisbet, E.G. (1982) Komatiites. George Allen & Unwin, London, 526 p.

[42] Sproule, R.A., Lesher, C.M., Ayer, J.A., Thurston, P.C. and Herzberg, C.T. (2002) Spatial and Temporal Variations in the Geochemistry of Komatiites and Komatiitic Basalts in the Abitibi Greenstone Belt. *Precambrian Research*, **115**, 153-186. https://doi.org/10.1016/S0301-9268(02)00009-8

[43] Mandal, S., Robinson, D.M., Kohn, M.J., Khanal, S., Das, O., and Bose, S (2016) Zircon U-Pb Ages and Hf Isotopes of the Askot Klippe, Kumaun, Northwest India: Implications for Paleoproterozoic Tectonics, Basin Evolution and Associated Metallogeny of the Northern Indian Cratonic Margin. *Tectonics*, **35**, 965-982. https://doi.org/10.1002/2015TC004064

[44] Hanson, G.N. and Langmuir C.H. (1978) Modelling of Major Elements in Mantle-Melt Systems Using Trace Element Approaches. *Geochimica et Cosmochimica Acta*, **42**, 725-74. https://doi.org/10.1016/0016-7037(78)90090-X

[45] Herzberg, C. and O'Hara, M.J. (2002) Plume-Associated Ultramafic Magmas of Phanerozoic Age. *Journal of Petrology*, **43**, 1857-1883. https://doi.org/10.1093/petrology/43.10.1857

[46] Hollocher, K., Robinson, P., Walsh, E. and Roberts, D. (2012) Geochemistry of Amphibolite-Facies Volcanics and Gabbros of the Støren Nappe in Extensions wEst and Southwest of Trondheim, Western Gneiss Region, Norway: A Key to Correlations and Paleotectonic Settings. *American Journal of Science*, **312**, 357-416. https://doi.org/10.2475/04.2012.01

[47] Jochum, K.P., Arndt N.T. and Hofman A.W. (1991) Nb-Th-La in Komatiites and Basalts: Constraints on Komatiite Petrogenesis and Mantle Evolution. *Earth and Planetary Science Letters*, **107**, 272-289. https://doi.org/10.1016/0012-821X(91)90076-T

[48] Woodhead, J.D. and Johnson, R.W. (1993) Isotopic and Trace-Element Profiles Across the New Britain Island Arc, Papua New Guinea. *Contributions to Mineralogy and Petrology*, **113**, 479-491. https://doi.org/10.1007/BF00698317

[49] Gamble, J.A., Wright, I.C., Woodhead, J.D. and Smith, I. (1995) Arc and Back-Arc Geochemistry in the Southern Kermadec Arc-Ngatoro Basin and Offshore Taupo Volcanic Zone, SW Pacific. In: Smellie, J.L., Ed., *Volcanism Associated with Extension at Consuming Plate Margins*, Geological Society of Special Publication, London, 193-212. https://doi.org/10.1144/GSL.SP.1994.081.01.11

[50] Wang, C.Y., Zhang, Q., Qian, Q. and Zhou, M.F. (2005) Geochemistry of the Early Paleozoic Baiyin Volcanic Rocks (NW China): Implications for the Tectonic Evolution of the North Qilian Orogenic Belt. *The Journal of Geology*, **113**, 83-94. https://doi.org/10.1086/425970

[51] Pearce, J.A. and Stern, R.J. (2006) Origin of Back-Arc Basin Magmas: Trace Element and Isotope Perspectives. In: Christie, D.M., Fisher, C.R., Lee, S.-M. and Givens, S., Eds, *Back-Arc Spreading Systems: Geological, Biological, Chemical, and Physical Interactions*, Vol., 166, American Geophysical Union, Washington DC, 63-86. https://doi.org/10.1029/166GM06

[52] Bézos, A., Escrig, S., Langmuir, C.H., Michael, P.J. and Asimow, P.D. (2009) Origins of Chemical Diversity of Back-Arc Basin Basalts: A Segment-Scale Study of the

Eastern Lau Spreading Center. *Journal of Geophysical Research*: *Solid Earth*, **114**, Article No. B06212. https://doi.org/10.1029/2008JB005924

[53] Saha, A., Mudholkar, A.V., Kamesh Raju, K.A., Doley, B. and Sensarma, S. (2018) Geochemical Characteristics of Basalts from Andaman Subduction Zone: Implications on Magma Genesis at Intraoceanic Back-Arc Spreading Centres. *Geological Journal*, **54**, 3489-3508. https://doi.org/10.1002/gj.3345

[54] Pearce, T.H., Gorman, B.E. and Birkett, T.C. (1977) The Relationship between Major Element Chemistry and Tectonic Environment of Basic and Intermediate Volcanic Rocks. *Earth and Planetary Science Letters*, **36**, 121-132. https://doi.org/10.1016/0012-821X(77)90193-5

[55] Cabanis, B. and Lecolle, M. (1989) Le diagramme La/10-Y/15-Nb/8: Un outil pour la discrimination des séries volcaniques et en évidence des mélanges et/ou de contamination crustale. *Comptes Rendus de l'Académie des Sciences*, *Série II*, **309**, 2023-2029.

[56] Tchameni, R. (1997) Géochimie et géochronologie des formations de l'Archéen et du Paléoprotérozoïque du Sud-Cameroun (groupe du Ntem, Craton du Congo). Université d'Orléans, Orléans, 356 p.